Angewandte Chemie International Edition
www.angewandte.org

How to cite: *Angew. Chem. Int. Ed.* **2024**, *63*, e202416039
doi.org/10.1002/anie.202416039

Coupled Photocatalysis

Coupling Photocatalytic Hydrogen Production with Key Oxidation Reactions

Jiayan Teng[+], *Wenlu Li*[+], *Zhen Wei*,* *Derek Hao, Lin Jing, Yuxi Liu, Hongxing Dai, Yongfa Zhu, Tianyi Ma*,* *and Jiguang Deng**

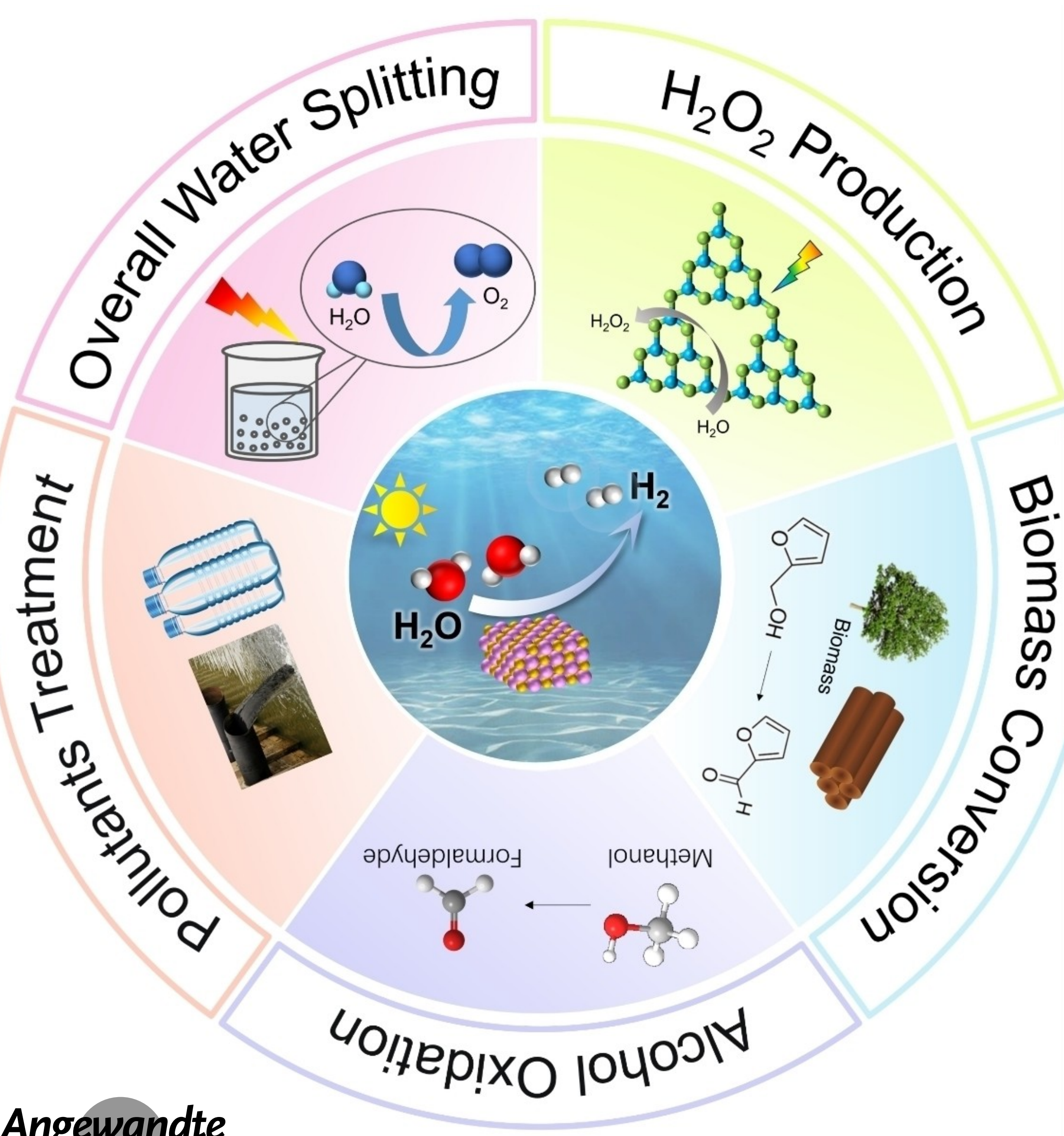

Abstract: Hydrogen represents a clean and sustainable energy source with wide applications in fuel cells and hydrogen energy storage systems. Photocatalytic strategies emerge as a green and promising solution for hydrogen production, which still reveals several critical challenges in enhancing the efficiency and stability and improving the whole value. This review systematically elaborates on various coupling approaches for photocatalytic hydrogen production, aiming to improve both efficiency and value through different oxidation half-reactions. Firstly, the fundamental mechanism is discussed for photocatalytic hydrogen production. Then, the advances, challenges, and opportunities are expanded for the coupling of photocatalytic hydrogen production, which focuses on the integration of value-added reactions including O_2 production, H_2O_2 production, biomass conversion, alcohol oxidation, and pollutants treatment. Finally, the challenges and outlook of photocatalytic H_2 production technology are analyzed from the aspects of coupling hydrogen production value, photocatalyst design and reaction system construction. This work presents a holistic view of the field, emphasizing the synergistic benefits of coupled reactions and their practical application potential, rather than focusing on catalysts or single reaction systems. This review provides valuable references for the development and application of photocatalytic hydrogen production in energy conversion and environmental conservation through sustainable, eco-friendly and economic pathways.

1. Introduction

Our society is facing the dual challenges of an energy crisis and environmental pollution. The traditional energy paradigm falls short of meeting the soaring energy demands and concurrently imposes considerable environmental damage.[1] Therefore, the development of clean and sustainable energy has become a global consensus. In react years, hydrogen (H_2) has attracted enormous attention as an efficient and environmentally friendly energy medium. Compared with traditional energy sources, the combustion of H_2 only generates water and energy without producing any pollutants.[2] However, current H_2 production mainly relies on fossil fuels, which is incompatible with the concept of environmental protection.[3] Therefore, it is crucial to explore green and renewable H_2 production technologies. Photocatalytic H_2 production from water splitting is considered a key technology for future sustainable energy solutions.[4] The principle of photocatalytic H_2 production involves using solar energy to excite electrons inside the semiconductor catalyst material, activating the surface, and catalyzing the photolysis reaction of water molecules to yield H_2 and O_2. This process does not require an external power source and has environmentally friendliness and efficient characteristics.[5]

However, the photocatalytic hydrogen production from water splitting is only a reduction half-reaction, which requires proper oxidation half-reactions to complete the entire reaction. Some value-added reactions can be coupled to improve the energy utilization and economic value of the photocatalytic hydrogen production reaction, achieving a win-win situation.[6] Such multifunctional photocatalytic systems include the reaction coupling with O_2 production, H_2O_2 production, biomass conversion, alcohol oxidation, degradation of organic pollutants, and so on. The synthesis of H_2O_2 via water splitting confers a chemical that is highly valued in market and industrial contexts.[7] The coupling of biomass conversion and alcohol oxidation can produce higher–value products as well as increase reaction rates. And the coupling with pollutant degradation exhibits a large perspective in environmental pollution control.[8] The coupling of these reactions depends on the design of the photocatalysts in band structure, active sites, and charge transfer pathways.

Previous reviews on photocatalytic hydrogen evolution reactions have primarily focused on specific aspects of the process. For instance, Lin et al. provided a comprehensive overview of catalyst materials for photocatalytic water splitting,[9] while Wang et al. focused on the mechanisms of charge separation in photocatalytic systems.[10] Lin et al. reviewed the progress in visible-light-driven photocatalytic

---

[*] J. Teng,[+] Dr. Z. Wei, L. Jing, Y. Liu, H. Dai, Dr. J. Deng
Beijing Key Laboratory for Green Catalysis and Separation, Key Laboratory of Beijing on Regional Air Pollution Control, Key Laboratory of Advanced Functional Materials, Education Ministry of China, Beijing University of Technology
Beijing 100124, China
E-mail: xfwz522@126.com
jgdeng@bjut.edu.cn

Dr. W. Li,[+] Y. Zhu
Department of Chemistry, Tsinghua University
Beijing 100084, China

Dr. W. Li[+]
School of Food and Health, Beijing Technology and Business University
Beijing 100048, China

D. Hao, Dr. T. Ma
Centre for Atomaterials and Nanomanufacturing (CAN), School of Science, RMIT University
Melbourne 3000, Australia
E-mail: tianyi.ma@rmit.edu.au

D. Hao, Dr. T. Ma
ARC Industrial Transformation Research Hub for Intelligent Energy Efficiency in Future Protected Cropping (E2Crop)
Melbourne 3000, Australia

[+] These authors contributed equally to this work: Jiayan Teng, Wenlu Li.

hydrogen production.[11] However, comprehensive reviews are notably absent which systematically examine the coupling of photocatalytic hydrogen production with various value-added reactions and environmental remediation processes.

In this review, we explore the frontier research on photocatalytic H_2 production coupled with value-added reactions, with a primary focus on the design of multifunctional photocatalytic systems and the optimization of photocatalysts. The review not only discusses the technological advances in this field but also considers the scalability and sustainability of these processes for real-world applications. This paper provides a comprehensive overview of the current research and future trends in photocatalytic H_2 production, which is valuable for both fundamental research and industrial implementation.

2. Mechanisms of Photocatalytic H_2 Production

Semiconductor photocatalysis typically involves irradiating semiconductor materials with light, prompting valence band (VB) electrons to absorb energy and excite to the conduction band (CB), creating corresponding holes. When these photogenerated electrons and holes are transferred to the surface of the materials, redox reactions will occurs with targeted molecules.[12] In general, the main steps for photocatalytic H_2 production are shown in Figure 1: (i) sunlight irradiation produces photogenerated electron–hole pairs (e^-, h^+); (ii) photogenerated electron–hole pairs separate and migrate to the surface, during which the excited state carriers may also competitively recombine within a few nanoseconds, releasing thermal energy; (iii) the carriers that have migrated to the surface react with adsorbed protons to produce H_2.[13]

$$2H^+ + 2e^- \rightarrow H_2,\ E\ (H^+/H_2) = 0\ V\ vs.\ RHE \qquad (1)$$

Overall water splitting is a key step in photocatalytic hydrogen production because it directly involves the decomposition of water molecules to produce hydrogen and oxygen. In the overall water splitting reaction, semiconductor materials typically need to have a specific band structure to meet the thermodynamic and kinetic requirements for water decomposition. Consequently, the band gap of the photocatalyst should theoretically exceed 1.23 V. As illustrated in

Jiayan Teng received her B.S. (2020) and M.S. degrees (2023) from Heilongjiang University. Now she is a Ph.D. student at Beijing University of Technology, working under the supervision of Prof. Jiguang Deng and Prof. Zhen Wei. Her research interest focuses on energy and environmental photocatalysis.

Dr. Wenlu Li received her B.S. (2018) and Ph.D. (2023) degrees from Tsinghua University under the supervision of Prof. Yongfa Zhu. Then she joined Beijing Technology and Business University as an assistant professor in 2023. Her current research interest focuses on photocatalytic water splitting.

Dr. Zhen Wei received his PhD in chemistry from Tsinghua University in 2019 under the supervision of Prof. Yongfa Zhu. Then he pursued his post-doctoral work at The University of Hong Kong. He joined Beijing University of Technology as a professor in 2023. His research interest focuses on semiconductor nanomaterials for photo/electro-catalytic applied in environment and energy chemistry.

Dr. Tianyi Ma is a Distinguished Professor in RMIT University, an Australian Research Council Future Fellow, Fellow of Royal Society of Chemistry, and Clarivate's Global Highly Cited Researcher in both Materials Science and Chemistry fields. He is a leading scientist in renewable energy field, with pioneering work in the areas of functional photocatalytic, electrocatalytic and piezocatalytic materials for renewable energy conversion. He was awarded Australian Acadmey of Science Le Févre Medal and Young Tall Poppy Science Award.

Dr. Jiguang Deng received his B.S. degree from Kunming University of Science and Technology in 2005. He subsequently obtained his PhD degree from Beijing University of Technology in 2010. He is a full professor in Beijing University of Technology. His research interests focus on environmental catalysis and clean energy applications.

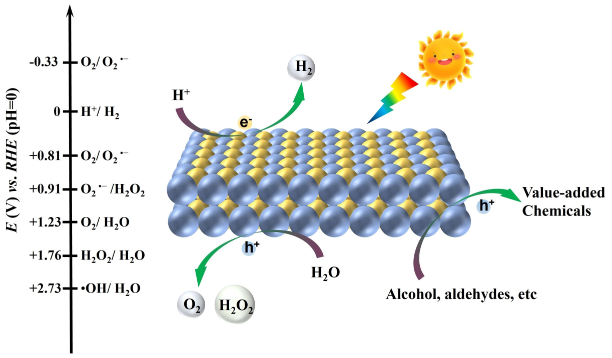

Figure 1. Schematic diagram of photocatalytic hydrogen production coupled with other reactions.

Figure 1, the potential of conduction band minimum (CBM) must be more negative than that of H^+/H_2 for H_2 production, and the valence band maximum (VBM) must be more positive than that of O_2/H_2O to enable oxygen production, to ensure that photogenerated charge carriers can oxidize and reduce water molecules.

$$2H_2O \rightarrow O_2 + 4e^- + 4H^+,\ E\ (O_2/H_2O) = +1.23\ \text{V}\ vs.\ \text{RHE} \tag{2}$$

In addition to the traditional four–electron oxidation reaction in water splitting, the generation of H_2 and H_2O_2 by the two-electron oxidation process is also a promising method.[14] The reaction of water splitting to produce H_2 and H_2O_2 is shown in equation 3, where the oxidation potential of H_2O_2/H_2O is 1.76 V. Therefore, compared with the four–electron process, two–electron water oxidation requires higher energy, which means the VBM of the photocatalyst needs to be corrected, which is thermodynamically unfavorable. However, the kinetic advantages of the two–electron process make it compete with the four–electron process.[15] Through the screening of catalysts, it becomes a possible method to produce H_2 and H_2O_2 simultaneously through water splitting. The schematic diagram is shown in Figure 1.

$$2H_2O \rightarrow H_2O_2 + H_2 \tag{3}$$

As discussed above, the oxidation reactions of water exhibit high energy barrier, which imposes stringent requirements on the structure of the catalysts. Consequently, some organic oxidation reactions reveal great potential on the coupling with H_2 production, which show lower energy barriers and circumvent the separation of H_2 and O_2 gas. Similar to overall water splitting, the first step is the photoexcitation of semiconductors and generation of excited electron–hole pairs, followed by the separation and migration of photogenerated charges. The electrons will react with proton to produce H_2, while the holes can make a direct oxidation of organic molecules to achieve higher value. Unlike overall water splitting process, the proton source for H_2 production reactions is also associated with organic substrates from some active functional groups (e.g., –OH, –COOH, $–NH_2$).[16] In this process, the hole oxidation induces bond cleavage in organic matter, producing protons and free radical intermediates. Protons engage in reduction reactions to yield H_2, while free radical intermediates recombine to form value–added products.[17] The alternative organic substrates for the coupled oxidation half reaction include biomass, alcohols, plastic polymers, organic dyes, antibiotics, and phenols, which can be converted into value-added or less harmful byproducts, such as glucose, organic acids, CO_2, and H_2O. These organic reactions also face some challenges, such as selectivity of productions, poor contact between solid polymers and catalysts, and mineralization of some organic pollutants.

3. Photocatalytic H_2 Production Coupling with O_2 Production

The process of photocatalytic H_2 production coupled with O_2 generation entails the complete photocatalytic water splitting to yield H_2 and O_2 in a molar ratio of 2:1. Despite its promise, this process faces several challenges, including low efficiency, side reactions, reverse reactions, and the separation of H_2 and O_2, which impede its practical application.[12a] Consequently, continuous research and development efforts are necessary to address these issues. This section aims to provide a comprehensive overview of the current understanding of the mechanisms involved, the challenges encountered, the strategies employed for optimization, and the future trends in the field. Table 1 presents a comparison of catalysts that exhibit competitiveness in water splitting.

3.1. Overall Water Splitting

The incorporation of a proper co–catalysts on semiconductor photocatalysts can significantly improve the catalytic performances by providing active sites that accelerate the reaction rate. Additionally, the interface created between the cocatalyst and the semiconductor photocatalyst facilitates charge separation and migration, which is crucial for improving photocatalytic efficiency. Noble metals, such as Pt,[28] Pd,[29] Rh, and Au,[30] are commonly used as co–catalysts due to their ability to increase the H_2 evolution rate, thereby boosting the overall photocatalytic performance. The O_2 production involves a four–electron transfer process, which is the rate–limiting step in the overall water splitting. The introduction of suitable oxygen evolution co–catalysts can reduce the activation energy barrier of the reaction, thus achieving a higher oxygen evolution rate. Commonly used oxygen evolution co–catalysts include IrO_2 and RuO_2, as well as metal oxides such as MnO_x, NiO_x, and CoO_x.[31] Chen et al. investigated the impact of loading Pt, Rh_2O_3, and NiO nanoparticles onto $Bi_{0.5}Y_{0.5}VO_4$ as co–catalysts on overall water splitting. Pt demonstrated better electron capture capabilities due to its larger work function. However, the addition of Pt co–catalysts did not effectively decrease the overpotential for O_2 evolution, decreasing the photocatalytic water splitting efficiency. On the other hand, NiO co–

Table 1: Comparison of photocatalytic properties of overall water splitting.

Catalysts	co–catalyst	Light	H_2 rate ($\mu mol\,h^{-1}\,g^{-1}$)	O_2 rate ($\mu mol\,h^{-1}\,g^{-1}$)	AQY	STH	Ref.
COF-SCAU-2	Pt	$\lambda > 420$ nm	46	21	10.23 %/420 nm	/	[18]
g-C_3N_4-D2	Pt, 3 %Co_3O_4 NRs	$\lambda > 420$ nm	49.6	24.71	11.94 %/400 nm	1.48 %	[19]
g-C_3N_4/rGO/PDIP	Pt, $Co(OH)_2$	$\lambda > 420$ nm	632	312	4.94 %/420 nm	0.30 %	[20]
Ni_2P/NiS@PCOS	/	$\lambda > 420$ nm	1507	702	7 %/420 nm	0.91 %	[21]
$BDCNN_{350}$/$BDCNN_{425}$	Pt, $Co(OH)_2$	$\lambda > 300$ nm	629	312.5	11.76 %/420 nm	1.16 %	[22]
CNN/BDCNN	Pt, $Co(OH)_2$	$\lambda > 300$ nm	823.5 ($\lambda > 300$ nm) 246.25 ($\lambda > 420$ nm)	410.5 ($\lambda > 300$ nm) 122 ($\lambda > 420$ nm)	5.95 %/400 nm 4.59 %/420 nm	/	[22]
CDots-C_3N_4	/	$\lambda > 420$ nm	105	51.3	16 %/420 nm	2.00 %	[23]
3D g-C_3N_4 NS	Pt, IrO_2	$\lambda > 420$ nm	102	51	1.4 %/420 nm	0.06 %	[24]
$ZnIn_2S_4$-WO_3/C-wood	Pt, CoO_x	air mass 1.5 light	4834	2357	21.63 %/380 nm	1.52 %	[25]
Fe_2O_3-C_3N_4/C-wood	Pt	air mass 1.5 light	3563	1768	16.05 %/380 nm	1.12 %	[25]
$SrTiO_3$: Al	Rh/Cr_2O_3, CoOOH	300 W Xe lamp	28000	14000	95.7 %/350 nm	0.65 %	[26]
$SrTiO_3$/$BiVO_4$	Ru, RuO_x	$\lambda > 420$ nm	4750	2350	30 %/419 nm	1.10 %	[27]

[a]: "/" in the table indicates that the data is not available.

catalysts exhibited less efficient separation of electrons and holes but successfully reduced the overpotential for O_2 evolution, leading to a substantial enhancement in photocatalytic activity. In comparison to Pt and NiO, Rh_2O_3 co–catalysts not only effectively promoted the separation of photogenerated electron–hole pairs but also reduced the overpotential for O_2 evolution (0.13 V). Consequently, $Bi_{0.5}Y_{0.5}VO_4$ loaded with Rh_2O_3 exhibited the highest overall water splitting photocatalytic activity.[32]

Visible light makes up about 43 % of the solar spectrum, underscoring the importance of creating catalysts that can harness visible light to improve the utilization of solar energy. However, the photocatalytic activity of single-component material is limited by either the light absorption range or the capability for overall water splitting. Therefore, the combination of two materials in Z-Schemes can address this limitation. This approach leverages efficient electron transport within the Z-Scheme system, which is instrumental in promoting the spatial separation of electrons and holes, thereby optimizing the photocatalytic process.[33] Qi et al. designed a Z-scheme system with ZrO_2-modified TaON as a H_2 evolution catalyst, where $BiVO_4$ supported by Ir and $FeCoO_x$ were used as oxygen evolution catalyst, and $[Fe(CN)_6]^{3-/4-}$ was used as electron transport medium. The apparent quantum yield (AQY) of this configuration reached 12.3 % at 420 nm.[34] Wang et al. designed a novel photothermally–photocatalyzed Z-scheme overall water splitting system, using surface carbonized wood as the electron transport medium (Figure 2b). The photothermal effect was utilized to convert liquid water into steam, inhibiting carrier recombination and reducing the reaction barrier, leading to a solar-to-hydrogen (STH) efficiency of 1.52 %.[25] In addition, Sasaki et al. proved for the first time Ru/$SrTiO_3$ and Rh-$BiVO_4$ particles exhibit opposite charges under pH = 3.5, achieving close bonding through electrostatic action, provide effective contact for electron transfer between particles, which resulted in an AQY value of 1.7 % at 420 nm.[35]

Graphite–phase carbon nitride (g-C_3N_4), a two–dimensional layered non–metallic organic polymer semiconductor first reported by Wang et al. in 2009, exhibits a response to visible light, making it a subject of extensive research due to its tunable band structure, stability, and straightforward synthesis.[36] For further optimization the catalytic efficiency of g-C_3N_4, nano–structure design and the construction of heterogeneous structures are usually used to improve the catalytic activity. Shen et al. designed a g-C_3N_4 nanosheet with a continuously tunable band structure containing boron impurities/nitrogen defects. The Z-scheme heterostructure of g-C_3N_4-based 2D/2D was constructed by electrostatic self-assembly. In the presence of co–catalyst, the solar–hydrogen energy conversion efficiency reached 1.16 %.[22] Zhu et al. constructed a new polymer Z-scheme heterostructure g-C_3N_4/rGO/Perimide Polymer (g-C_3N_4/rGO/ PDIP). rGO/PDIP nanorods were obtained by coating a layer of rGO on the surface of PDIP nanorods through a wet chemical reduction process. The resulting product was then loaded onto g-C_3N_4 nanosheets by solvent volatilization and deposition method, followed by heat treatment to obtain g-C_3N_4/rGO/PDIP heterostructure photocatalyst (Figure 2d). The Z-scheme exhibited a substantial internal electric field, which significantly enhanced the charge separation efficiency. Femtosecond transient absorption spectroscopy showed that the hole lifetime of PDIP at heterojunction was extended to 201.7 ns, while the electron lifetime was reduced to 14.1 ns compared with bare PDIP. The results suggest efficient space charge transfer within heterogeneous structures, where photogenerated electrons from PDIP are rapidly transferred to g-C_3N_4 via rGO, whereas photogenerated holes remain longer in PDIP, avoiding recombination. With Pt/Cr_2O_3 as co–catalyst, the photocatalytic overall water splitting achieved nearly 12 times the H_2 and O_2 yield of g-C_3N_4 nanosheets, and reaching an AQY of 4.94 % at 420 nm (Figure 2e).[20]

In addition to g-C_3N_4, several other organic polymers have been used in photocatalytic systems. Examples include covalent triazine frameworks (CTFs), conjugated microporous polymers (CMPs), and covalent organic skeleton materials (COFs), covalent triazine framework (CTFs), which is distinguished by an extremely large π conjugation and a unique arrangement.[37] Yang et al. studied the photocatalytic overall water splitting activity of β–ketoamine covalent

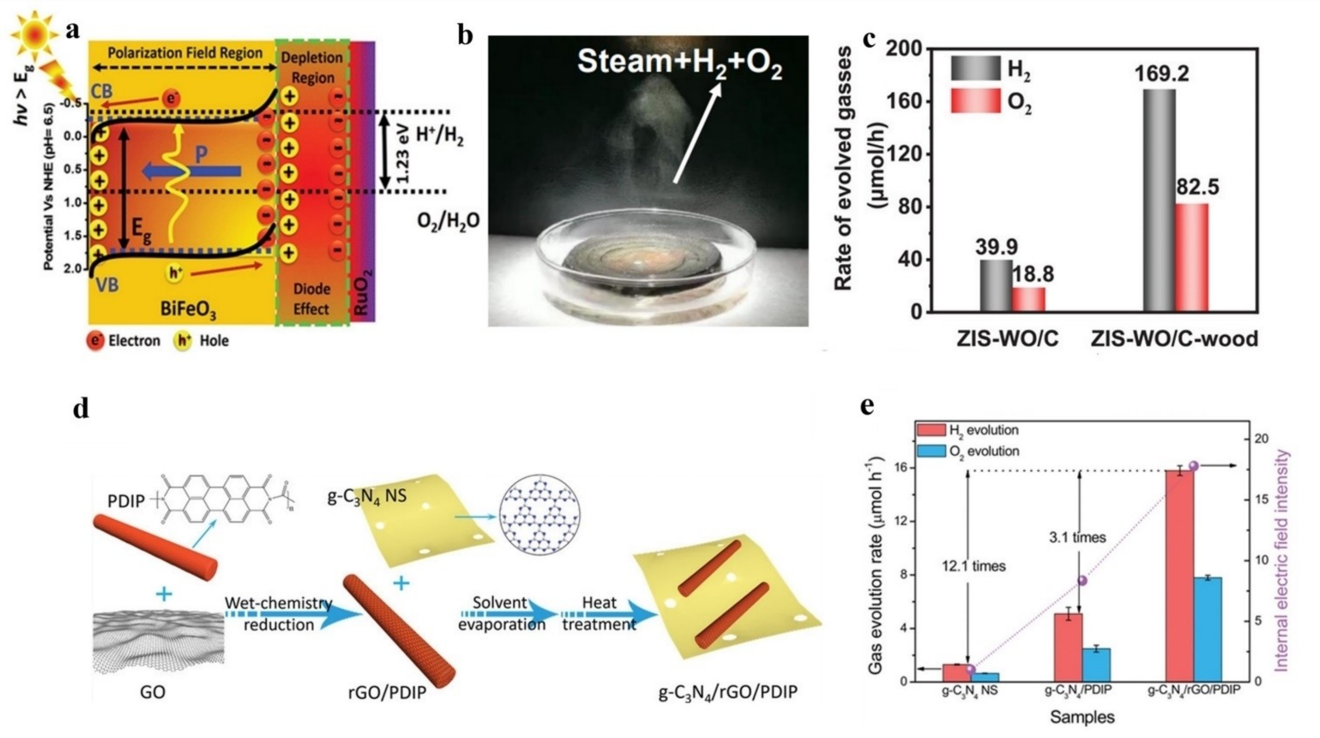

Figure 2. (a) Scheme of $RuO_2/BiFeO_3$ photocatalytic overall water splitting mechanism. Reprinted with permission.[31] Copyright 2020, Wiley-VCH. (b) ZIS-WO/C wood produces steam, H_2 and O_2 under simulated sunlight. (c) H_2 and O_2 evolution rates of ZIS-WO/C (carbon powder) and ZIS-WO/C-wood system. Reprinted with permission.[25] Copyright 2021, Wiley-VCH. (d) The synthesis schematic illustration and (e) overall water splitting activity of g-C_3N_4/rGO/PDIP samples. Reprinted with permission.[20] Copyright 2021, Wiley-VCH.

organic framework by systematically regulating the N site, structure and morphology. The Pt@TpBpy-NS and Pt@TpBpy-2-NS both exhibit visible-driven water decomposition activity after the introduction of subnanometer platinum (Pt) nanoparticles as co–catalysts in the pores of COFs nanosheets. The best H_2 and O_2 yields of Pt@TpBpy-NS were 9.9 and 4.8 μmol/5 h, respectively, and the maximum STH was 0.23 %. Further mechanistic studies revealed that small differences in N sites in COFs led to significant differences in electron transfer and reaction barriers.[37d]

Since achieving photocatalytic overall water splitting with the NiO-$SrTiO_3$ system for the first time in 1982, Domen's team has been committed to optimizing the performance of $SrTiO_3$ semiconductor materials through photocatalytic design strategies.[38] In 2020, Domen's team doped $SrTiO_3$ with Al ($SrTiO_3$: Al) to mainly reduce the Ti^{3+}defect concentration. Concurrently, they utilized crystal surface design engineering to selectively deposit the co–catalysts Rh/Cr_2O_3 and CoOOH on specific crystal facets, thereby increasing the efficiency of H_2 and O_2 evolution reactions. Additionally, the molten salt method was applied to $SrTiO_3$: Al to enhance crystallization and carrier transport properties. These combined strategies resulted in a quantum efficiency of 96 % for UV light in the 350–360 nm.[39]

Currently, the practical application of photocatalytic H_2 production technology is limited by its low STH. Mi et al. crafted InGaN/GaN nanowire photocatalysts on commercial silicon wafers with high crystallinity and a broad visible light response range using molecular beam epitaxy growth techniques. This approach led to an impressive STH efficiency of up to 9.2 %. To facilitate large–scale applications, a lens, comparable in size to a house window, precisely concentrates sunlight onto an experimental panel just a few inches wide. Remarkably, the InGaN/GaN nanowires, implemented on 4 cm ×4 cm commercial silicon wafers, exhibit exceptional stability under conditions of high light intensity and elevated temperatures. Furthermore, these nanowires demonstrate an average STH efficiency of 6.2 %, representing the highest efficiency achieved to date for such a natural photocatalytic total water reaction system. It also provides the possibility for the industrial application of photocatalytic overall water splitting devices (Figure 4d).[40]

3.2. Seawater Splitting

Since seawater constitutes approximately 97 % of the water resources of the earth, photocatalytic splitting of seawater to produce H_2 is more cost effective and environmentally friendly, compared with pure water. However, seawater has complex composition, which includes a variety of inorganic salts, organic matter, and microorganisms, poses significant challenges for photocatalysis. Specifically, the high concentration of Cl^- in seawater can lead to the deactivation of photocatalysts and the consumption of photogenerated carriers, thereby diminishing the photocatalytic activity. This interaction is often represented by a series of equations, such as equations (4–7), which detail the photochemical reactions involved.[41] Therefore, it is important to improve the tolerance to Cl^- of catalysts for photocatalytic seawater splitting. The design concept of catalysts mainly includes decreasing the adsorption of Cl^- on the catalyst surface, reducing the VB potential to inhibit he oxidation of Cl^-, and even using Cl^- to regulate the charge polarization of catalysts.

$$Cl^- + h^+ \rightarrow \bullet Cl \tag{4}$$

$$\bullet Cl + e^- \rightarrow Cl^- \tag{5}$$

$$Cl^- + Cl\bullet \rightarrow Cl\bullet_2{}^- \tag{6}$$

$$Cl\bullet_2{}^- + e^- \rightarrow 2Cl^- \tag{7}$$

The most widely used catalyst in photocatalytic seawater splitting is still based on TiO_2.[41c,46] Micro and nano TiO_2 materials are usually selected, with CdS used for modification, and simulated seawater is generally employed for study. The co–catalyst can efficiently separate the electrons and holes. RuO_2 can be stabilized in NaCl and accelerate the electron transport, avoiding the influence of Cl^- on the H_2 production process.[47] However, Cl^- does not inevitably exert a negative effect on the reaction process. The experimental results of Li et al. show the increase in NaCl concentration leads to the enhancement of water splitting activity without the generation of Cl_2 or HClO.[47]

Several emerging catalysts are also being used to produce H_2 from seawater. Carbon nanodots (CNDs) serve as a universal alternative integrated into the photocatalytic HER scheme.[48] They exhibit high emission quantum yield, water solubility and seawater solubility, and biocompatibility.[49] Bikash Jana et al. synthesized pCNDs using citric acid and urea as raw materials by microwave assisted method, photo-oxidation was performed under air conditions. The optimized oCND-2 is used as catalysts in distilled water and seawater, the hydrogen formation rates in water and seawater are 15.15 and 19.70 $\text{mmol}\,g_{cat}{}^{-1}\,h^{-1}$, respectively. Its catalytic activity is highest when the $pH=8$ (close to the pH of seawater) (Figure 3c).[44] It has also been reported that carbon dots (CDs) are modified on hollow tube carbon nitride, and CDs acts as an active site for photothermal catalytic H_2 evolution and photo–induced heat source for accelerating electron diffusion. Photocurrent response curves and electrochemical impedance tests at different temperatures show that the introduction of CDs and higher temperature can reduce the resistance and effectively inhibit the photoinduced electron–hole pair recombination, thereby improving H_2 production activity.[50]

COFs are crystalline and porous, which are constructed through the linkage of covalently bonded building units. The 2D structure of COFs ensures the delocalization of charge in the conjugated frame, which is conducive to charge separation and migration, and the layered sheet structure can respond quickly to light excitation (Figure 3b).[43] Recently, Li et al. successfully designed and synthesized two kgm topologic oligo (phenylenevinylene) (OPV)–based COFs to promote photocatalytic H_2 production. Such a structural design results in the expansion of π–conjugation, accelerating the separation and transport of charge carriers. Additionally, the OPV fragments connected by the point generate more carriers under UV/Visible light irradiation, thereby enhancing the photocatalytic performance (Figure 3e–f).[45]

3.3. Scaling Up of Water Splitting

Despite laboratory advancements, the large-scale application of overall photocatalytic water splitting for H_2 production still faces several challenges. Traditional powder photocatalysts are often limited by some challenges, such as aggregation, hard recovery, poor accessibility to gaseous reactants all of which significantly hinder their large-scale application. Additionally, due to the low energy density of solar radiation, the scalability and efficiency of devices used for water photolysis are equally crucial. Taeghwan Hyeon et al. tackled these challenges by developing a buoyant photocatalytic platform made from a porous elastomer–hydrogel nanocomposite.[51] Positioned at the air–water interface, these nanocomposites exhibit efficient light transmission, rapid water supply, and immediate gas separation. Consequently, even without forced convection, the Pt/TiO_2 aerogels enable a substantial H_2 evolution rate of 163 $\text{mmol}\,h^{-1}\,m^{-2}$. The authors additionally demonstrate the scalability of floating photocatalytic nanocomposites. Employing Cu SA/TiO_2 NP as a photocatalyst, they crafted an array of nanocomposites covering a total area of 1 m^2. In natural sunlight averaging an intensity of 0.732 $kW\,m^{-2}$, a 1 m^2 nanocomposite generates 79.2 ml of H_2 daily.

In 2018, Domen et al. used $SrTiO_3$: Al as the photocatalyst to achieve a 1 m^2 photodecomposition aquatic H_2 device. During trials conducted under natural sunlight in September in Tokyo, the device exhibited the production of numerous bubbles. These bubbles could be smoothly discharged and collected through the air vent at the upper end of the reactor. By calculation, the conversion efficiency of sunlight reached 0.4 %.[52] Moreover, in 2021, Domen reported the implementation of a 100 m^2 panel reactor array incorporating a commercial polyimide membrane. This advanced system is designed to autonomously recover H_2 from a wet gas product mixture, ensuring safe and continuous operation over several months (Figure 4a–c).[39] The researchers optimized the system to obtain higher safety and durability, so that when intentionally ignited to recover H_2, the reactor remained intact, reaching a STH of 0.76 %. Although H_2 production efficiency is still not high enough for industrial application, it demonstrates the feasibility of safe, large–scale photocatalytic water splitting of H_2 production and gas collection separation.

Li et al. drew inspiration from the Z-scheme natural photosynthesis system, which spatially separates Photosystem II and Photosystem I, as well as the spatial separation of light reactions and dark reactions.[53] They utilized the identical principle for the spatial segregation of the water oxidation and proton reduction reactions within the water splitting process. By precisely controlling the exposure ratio of the

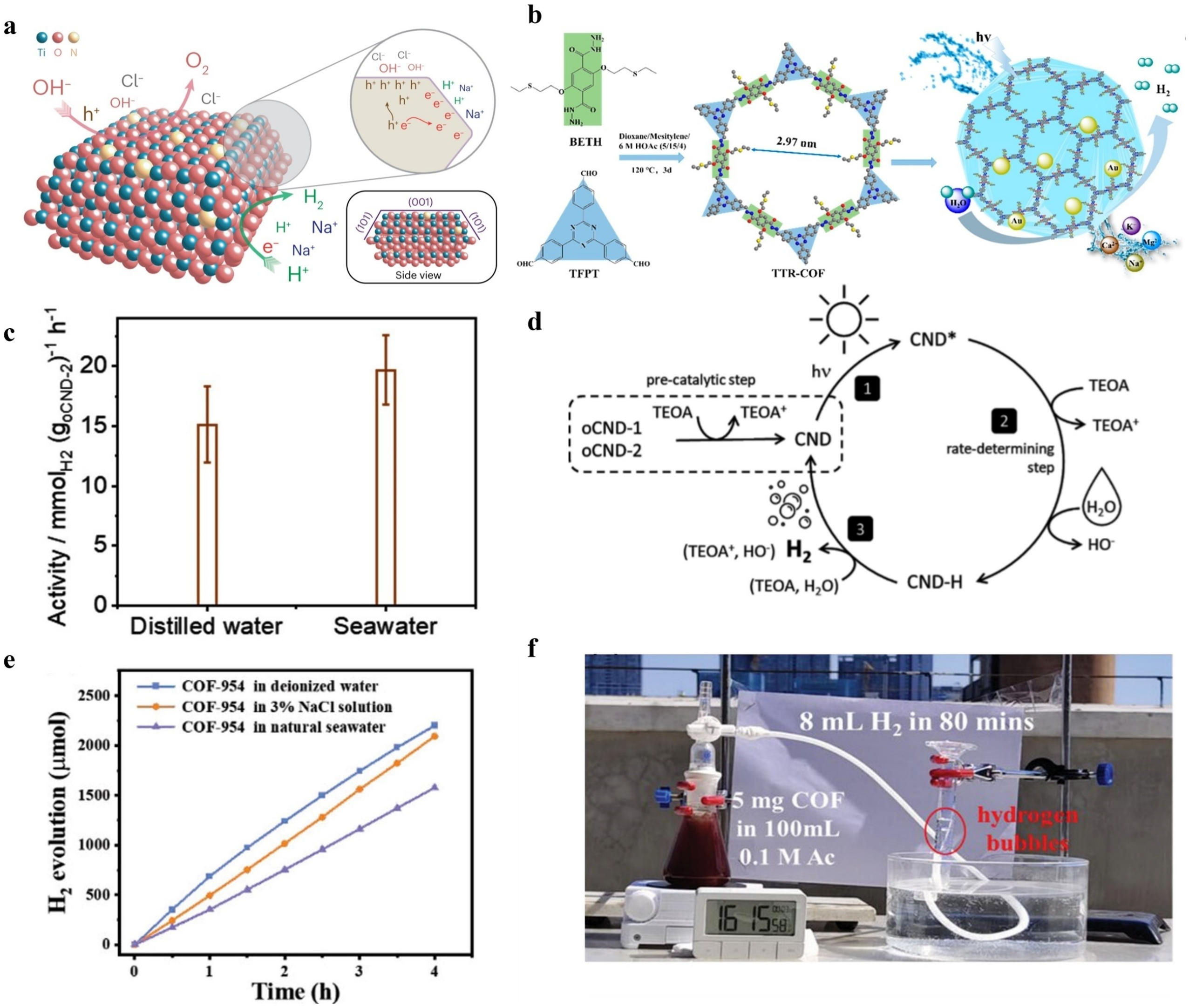

Figure 3. (a) Scheme of the electrolyte-assisted charge polarization of the facet-controlled N–TiO_2 in photocatalytic seawater splitting. Reprinted with permission.[42] Copyright 2024, Springer Nature. (b) Synthesis principle of TRR–COF and its application in seawater photocatalytic H_2 production. Reprinted with permission.[43] Copyright 2019, American Chemical Society. (c) Photocatalytic H_2 production rates of pure water and seawater (d) Catalytic cycle describing hydrogen evolution reaction activity of the photo oxidized CND materials. Reprinted with permission.[44] Copyright 2021, American Chemical Society. (e) Photocatalytic H_2 evolution under visible light and (f) photocatalytic equipment of COF-954 with 5 wt% Pt. Reprinted with permission.[45] Copyright 2023, Wiley-VCH.

oxidation and reduction reaction facets of $BiVO_4$ photocatalyst, they optimized the performance of photocatalytic water oxidation. Under the conditions of Fe^{3+}/Fe^{2+} ions serving as the energy storage medium, the visible light photocatalytic quantum efficiency for water oxidation reaches 71%. The STH of the "Hydrogen Farm" system exceeds 1.8%, which is currently the highest reported efficiency for converting solar energy to hydrogen based on powder nano–particle photocatalytic water splitting. The spatial separation of the water oxidation reaction and the proton reduction reaction in the water splitting process avoids the reverse reaction and circumvents the issue of separating the produced hydrogen and oxygen. The water oxidation reactor can operate in an open system without the need for sealing, thereby addressing the technological bottleneck for large–scale applications in principle.

When scaling up photocatalytic water splitting H_2 production systems, ensuring the safety and durability of the systems is critical. Due to the flammable nature of H_2 produced during the water splitting, strict safety measures must be taken, in addition to the design of the gas separation system, should also include the establishment of gas detection and leak alarm systems to prevent potential hydrogen leakage risks.

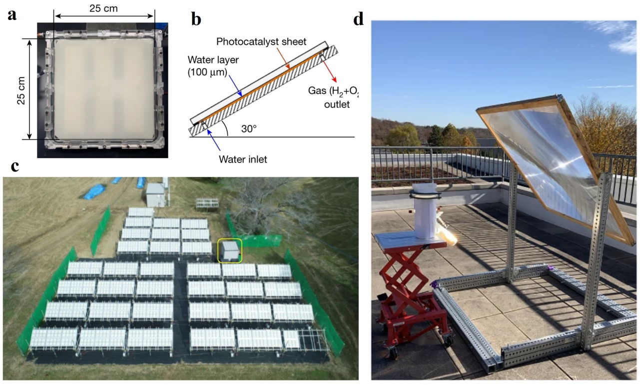

Figure 4. A 100 m^2 photocatalytic panel system for H_2 production. (a) Diagram and (b) side view of the panel reactor unit. (c) Top view of the whole photocatalytic panel system, containing1600 panel reactor units and a small house for gas separation (highlighted in the yellow box). Reprinted with permission.[39] Copyright 2021, Springer Nature. (d) Image of outdoor photocatalytic overall water splitting system. Reprinted with permission.[40] Copyright 2023, Springer Nature.

4. Photocatalytic H_2 Production Coupling with H_2O_2 Production

H_2O_2 is an important chemical building block, but the traditional anthraquinone–based production method requires multiple steps and is extracted from organic solvents, resulting in high energy consumption and environmental pollution.[54] Solar catalytic production of H_2O_2 is a promising method, generally through photocatalytic reduction of O_2 to produce H_2O_2. However, the simultaneous production of H_2 and H_2O_2 in the water decomposition process is less studied. Compared with traditional four–electron transfer processes, it is more ideal to convert water into H_2 and H_2O_2 through a two–electron pathway, with the value adding of all products. Furthermore, this approach circumvents separation challenges, with H_2 in the gas phase and H_2O_2 in the liquid phase, providing notable benefits over single water splitting. However, during the reaction process, the photocatalyst may also cause the decomposition of H_2O_2 to generate oxygen and water, which will reduce the H_2O_2 production rate.

At present, most photocatalysts are designed for either single H_2 evolution reaction or water oxidation/oxygen reduction reaction to produce H_2O_2. There is a pressing need for future research to focus on the development of stable catalysts that are capable of efficiently performing both processes concurrently. Piao et al. prepared Pt/TiO_2(anatase) as photocatalyst, in which anatase TiO_2 nanoparticles were synthesized by hydrothermal method. Subsequently, Pt/TiO_2 was obtained by photoreduction method for testing. H_2 and H_2O_2 generation rates reached 7410 and 5096 $\mu mol\,g^{-1}\,h^{-1}$, respectively. It is noteworthy that the H_2O_2 yield of the catalyst is much higher than that of Pt/P25 and Pt/C_3N_4.[55]

The g-C_3N_4 shows great potential in the field of photocatalytic overall water splitting, and the formation of H_2O_2 appears to compete thermodynamically with O_2 production.[56] Meanwhile, g-C_3N_4 cannot meet the thermodynamic requirements of H_2O_2 generation. Therefore, modification or the construction of a multi–component catalyst becomes essential to realize a two-electron water reforming path. Liu et al. reported a g-C_3N_4-based water reforming photocatalyst (PtO_x-RGO CN_x) comprising three components: hydroheat treated g-C_3N_4 (CN_x), reduced graphene oxide (RGO) and double co–catalysts (Pt and PtO_2). RGO can not only improve H_2 precipitation by increasing the carrier transfer rate, but also improve H_2 generation. The platinum co–catalyst can also be oxidized to a stable PtO_2 form while improving the overall stability.[57]

Optimizing the surface electronic structure of the catalyst can accelerate the surface catalytic reaction kinetics and improve the photocatalytic activity. Jiang et al. designed Ni–doped CoP nanoparticles anchored carbon phosphide nitride nanosheets (PCN-Ni-CoP) through an absorption–phosphating strategy, with the structure shown in Figure 5a. The H_2 and H_2O_2 production rate reached 124.3 and 447 $\mu mol\,g^{-1}\,h^{-1}$, respectively. The P element and the Co–N coordination interface made significant promotion for the separation and transfer of photogenerated charges in the interior and interface, offering valuable insights for catalyst design.[58]

Wei et al. modified Cu nanoparticles (NPs) onto TiO_2 hollow spheres for photocatalytic overall water splitting under UV and visible light. The Cu/TiO_2 metal/semiconductor junction can regulate the products of different reaction pathways by adjusting the wavelength of incident light. Under UV light, photogenerated electrons of TiO_2 are captured by Cu NPs at the Schottky interface to produce H_2, while photogenerated holes oxidate water into H_2O_2 at surface of TiO_2 through a two–electron reaction. Cu NPs act as a plasmonic unit, extending the photoresponse range to 590 nm, transferring hot electrons to TiO_2 to produce H_2, and the hot holes in Cu NPs undergo a four–electron reaction to produce O_2, thus achieving the overall water splitting photocatalytic process (Figure 5b).[59] Yang et al. proposed a two–site electron–hole enrichment nickel catalyst (Ni_2P/NiS@P-COS) by selecting a simplified kinetic pathway to optimize the thermodynamic energy barrier of water oxidation reactions. The results show that Ni_2P/NiS@PCOS can effectively optimize the thermodynamic and kinetic processes of overall water splitting. NiS efficiently captures photoexcited electrons from Ni_2P or PCOS and acts as an electron enrichment site to reduce H_2O to H_2. At the same time, the hole enrichment site at the Ni_2P/NiS@PCOS interface can oxidize H_2O to OH radical, further generating H_2O_2. By adding MnO_2, H_2O_2 can be decomposed into O_2 and H_2O. The catalytic activity of nickel catalysts can be effectively controlled by regulating the electron–hole enrichment state. This atomic level structure–activity interaction design provides a better understanding and guidance for other catalytic reactions.[21]

In photocatalytic process, the charge recombination rate is much faster than that of charge transfer and consumption.[61] Therefore, the rapid separation of the bulk phase charge after the photogenerated carrier formation is a necessary condition to improve the efficiency of solar energy conversion. For piezoelectric semiconductors with both piezoelectric and photocatalytic properties, the introduction of piezoelectric potential under light conditions is an effective strategy to promote bulk phase charge separation. While the

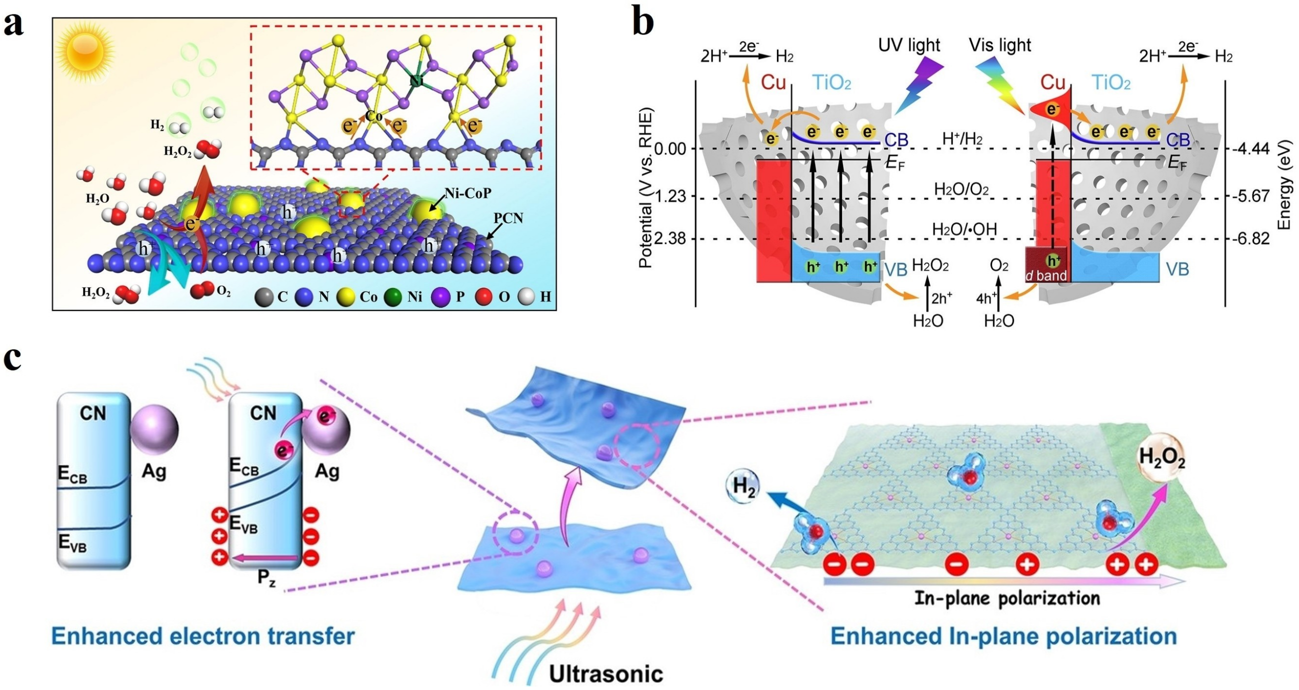

Figure 5. (a) The diagram of photocatalytic water splitting mechanism for PCN-Ni-CoP. Reprinted with permission.[58] Copyright 2023, Elsevier. (b) The mechanism diagram of Cu/TiO_2 in UV/Vis–driven photocatalytic overall water splitting. Reprinted with permission.[59] Copyright 2020, Elsevier. (c) Schematic mechanism of the piezocatalytic process. Reprinted with permission.[60] Copyright 2022, Wiley-VCH.

piezoelectric semiconductor generates electrons and holes under light, the piezoelectric polarized charge induced by mechanical stress can further promote the carrier separation.[62] Based on the above, Huang's team is committed to building an efficient piezoelectric catalytic system to achieve two–electron water decomposition to produce H_2 and H_2O_2. Graphite phase carbon nitride (CN) has stronger piezoelectric polarization and rich structural tunability than traditional inorganic piezoelectric bodies. Ag single atoms (SAs) and Ag clusters were successfully anchored to CN nanosheets simultaneously as multifunctional sites through a novel combined atomic limiting and post–reduction strategy, which realized efficient piezoelectric catalytic H_2 and H_2O_2 production (Figure 5c). This work combines theoretical calculations and microscopic techniques, confirming that Ag single atoms enhance the in–plane dipole and piezoelectric polarization of CN, while Ag clusters provide a strong interfacial electric field between CN and CN, together constructing an orthogonal charge transfer channel. In situ high voltage UV–visible diffuse reflectance spectroscopy and piezo–electrochemical tests revealed that Ag SAs and clusters increase electron density and decrease charge transfer impedance, and induce a a larger piezoresistive effect, thus improving carrier mobility.[60] Similarly, in 2023, the team reported the polar layered bismuth–rich bismuth–oxyhalide $Bi_4O_5X_2$ ($X=Br$, I) nanosheets as piezoelectric materials for piezoelectric catalytic pure water decomposition. This approach does not involve any cocatalyst and sacrificial agents. The piezoelectric catalytic decomposition of aquatic H_2 by $Bi_4O_5Br_2$ and $Bi_4O_5I_2$ thin layer nanosheets reached 1149.0 $\mu mol\,g^{-1}h^{-1}$ and 764.5 $\mu mol\,g^{-1}h^{-1}$, respectively, and the oxidation products are H_2O_2 and hydroxyl radical (•OH). Combining experiments and theoretical calculations, the mechanism of the different activity behind the two materials is explained. Compared with I element, the smaller radius and higher electronegativity of Br results in tighter polar crystal structure of $Bi_4O_5Br_2$, generating a larger dipole moment and a higher piezoelectric property, contributing to its better piezoelectric catalytic activity.[62b]

5. Photocatalytic H_2 Production Coupling with Biomass Conversion

The integration of biomass, a resource that is both extensive and renewable, is fundamental to mitigating the impact of greenhouse gas emissions and the gradual exhaustion of fossil fuel sources..[63] Combining biomass with photocatalysis offers an innovative path for environmental sustainability and renewable energy. Biomass based photocatalytic H_2 production follows the principle of water splitting, with the process continually refined for efficiency. Unlike traditional methods, biomass can hydrolyze, providing reducing groups that act as electron donors, eliminating the need for sacrificial agents and thus boosting hydrogen production rates. Dual-function catalysts represent a significant advancement in sustainable technology, as they have the capability to produce H_2 and selectively synthesize valuable chemicals. This dual functionality is a major step towards comprehensive solutions that address environmental challenges and enhance the utilization of renewable energy sources.[64] Up to now, the complex composition and structure of biomass still affects the conversion efficiency and selectivity, which limit the development and application of biomass.

5.1. Raw Biomass Conversion

Lignocellulose, constituting 90 % of biomass of similar plants on earth, stands out as the predominant renewable carbon resource, encompassing lignin, cellulose, and hemicellulose.[65] The conversion efficiency of lignocellulose into high–value chemicals hinges on the selective breaking of C–O or C–C bonds, especially under mild conditions.[66]

While natural lignin holds immense potential and application prospects as a vital biomass component, its intricate structure and chemically stable bonds have posed significant challenges to the conversion of lignin into valuable monomers.[71] Recent advancements reveal that CdS quantum dots serve as effective catalysts, facilitating the activation and breaking of β–O–4 bonds (C–O bonds) in lignin molecules. This photocatalytic reaction produces aromatic monomers (Figure 6a) under visible light at room temperature.[67,72] In this process, CdS quantum dots catalyze the oxidation and

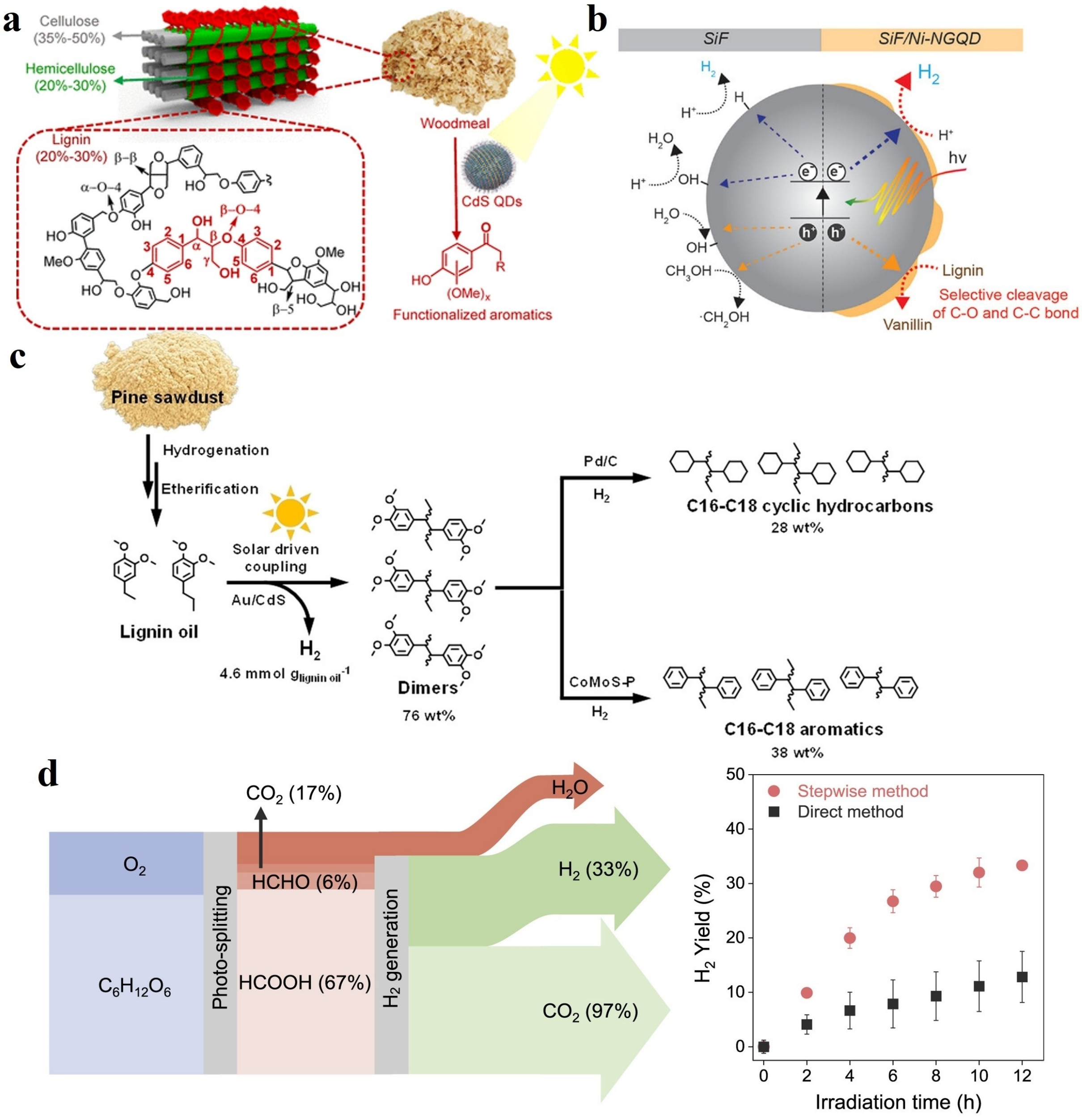

Figure 6. (a) Scheme of the structure and photocatalytic production of native lignin. Reprinted with permission.[67] Copyright 2019, American Chemical Society. (b) Scheme of solar biomass reforming with SiF and SiF/Ni-NGQD. Reprinted with permission.[68] Copyright 2023, Wiley-VCH. (c) The process of raw lignin to C16–C18 cyclic alkanes and aromatics. Reprinted with permission.[69] Copyright 2021, Wiley-VCH. (d) Stepwise comparison of photoassisted H_2 generation and direct photoreforming of glucose. Reprinted with permission.[70] Copyright 2023, Elsevier.

dehydrogenation of reactants, forming benzyl radical intermediates on the CdS surface through photogenerated holes. The energy of the intermediates β–O–4 bonds is substantially reduced, enabling easy acceptance of photogenerated electrons on the CdS surface. Consequently, the bonds are reduced, resulting in the formation of aromatic monomers. The theoretical yield of aromatic monomers from lignocellulose (such as birch powder) reaches an impressive 84 % under visible light. Remarkably, in the photocatalytic, the mild conditions of lignin conversion preserve cellulose and hemicellulose, ensuring their basic integrity. Further, through the hydrolysis of hemicellulose in solid products with weak acid, an 84 % yield of xylose is achieved. Simultaneously, enzymatic cellulose hydrolysis yields an outstanding 91 % glucose yield, marking a significant stride towards the comprehensive utilization of lignocellulose.

Soojin Park et al. has devised an innovative method for efficient H_2 production and biomass reforming, employing abundant and non–toxic photocatalysts. The approach utilizes low–gap silicon wafers (SiFs) as highly efficient light–absorbing materials. Then SiFs are modified with nickel–coordinated nitrogen–doped graphene quantum dots (Ni-NGQDs) to achieve the double harvest of biomass reforming and H_2 production with a high and stable efficiency. Under simulated sunlight conditions, the SiF/Ni-NQGDs catalyst demonstrated remarkable performance, yielding $14.2\ \mathrm{mmol\, g_{cat}}^{-1}\mathrm{h}^{-1}$ of H_2 and $147.1\ \mathrm{mg\, g_{lignin}}^{-1}$ vanillin, using sulfate lignin as the electron donor. Importantly, SiF/Ni-NQGDs can effectively prevent the deactivation of silicon through oxidation, ensuring sustained performance. Furthermore, it exhibits recyclability without apparent degradation in performance. This research offers significant understanding for the coupling of H_2 production and biomass refining using solar energy.[68]

Another method for lignin conversion involves depolymerizing the lignin into a phenolic mixture (lignin oil), and subsequently upgrading it into useful chemicals and liquid fuels, without the need for separation. In addition, utilizing lignin oil as a raw material has the potential to produce cycloalkanes and aromatics with higher energy densities than carbohydrate–derived biofuels, such as ethanol and alkanes. It is mainly composed of C8–C9 phenols, which can be convert to C8–C9 gasoline (alkanes or aromatics) via hydrodeoxidation. Dou et al. proposed a new route for preparing diesel oil from lignin oil in their study. Photocatalysis is employed to couple the monomers in lignin oil, generating dimer and H_2 at the same time. Subsequently, the dimers are converted to C16–C18 cycloalkanes or aromatics by hydrodeoxygenation (Figure 6c). Among several types of photocatalyst, Au/CdS shows high reactive activity to activated benzyl C–H bond. The introduction of Au improves the separation efficiency of photogenerated carrier and promotes the photocatalytic coupling reaction. Using 4-ethyl-1-methoxybenzene as substrate, Au/CdS produced dimer and H_2 with the rate of 2.4 and $1.6\ \mathrm{mmol\, g^{-1}\, h^{-1}}$, respectively. The feasibility of using pine wood as raw material to convert the primary material to diesel oil was demonstrated, which provided a new idea for lignin conversion.[69]

5.2. Biomass-Derived Molecules Conversion

Due to the complexity of biomass components, platform molecules are usually required as intermediates. Among these, biomass–derived furan compounds such as 5-hydroxymethylfurfural (HMF) and furfural stand out as pivotal platform molecules in the biorefinery process. These compounds possess the capability to be converted into a variety of value–added derivatives, thereby enhancing the versatility and economic viability of the biorefining processes.[73]

HMF can be oxidized into several high value–added derivatives due to the presence of the reactive functional groups: aldehyde (–CHO) and hydroxyl (–OH) groups. Among the derivatives of HMF, 2,5-diformylfuran (DFF) stands out as a key monomer in the production of medicine intermediates, organic conductors and functional polymers.[74] Solar–powered catalytic oxidation of HMF to DFF, accompanied by H_2 release, is considered as a promising method. Exploring active and stable photocatalysts remains challenging. It has been reported that flexible ultra–thin graphite carbon nitride (UCNT) has great potential. The UCNT catalyst exhibits high and stable performance in the selective oxidation of HMF to DFF, with the conversion rate of $95.0\ \mathrm{\mu mol\, g^{-1\, -1}}$ and selectivity of 95 % under visible light. The accompanied H_2 evolution rate is $29.0\ \mathrm{\mu mol\, g^{-1}\, h^{-1}}$. This effect is probably the result of a pronounced specific interaction between HMF and UCNT. The results of solid state nuclear magnetic resonance (NMR) and density functional theory (DFT) show that the twisted structure of HMF molecules engages robust interaction with UCNT, decreasing the energy barrier of dehydrogenation in HMF.[75] Besides, Mu et al. used a low cosolvent solvothermal method to synthesize NiS_2/CdS for visible light driven HMF conversion. NiS_2/CdS exhibits efficient HMF dehydrogenation to produce H_2 and DFF, with NiS_2 as a cocatalyst to accelerate the separation and transfer of photogenerated charges. The production rate of DFF and H_2 reach 519.64 and $476.60\ \mathrm{\mu mol\, g^{-1}\, h^{-1}}$, respectively.[76]

Photocatalytic conversion of carbohydrates into liquid hydrogen carriers (LHCs) for biomass H_2 production and storage is a highly promising approach. Wang et al. employed a "C–C bond first" strategy by first breaking the C–C bonds of carbohydrates on Ta-CeO_2 catalyst and converting them into C1 liquid hydrogen carriers composed of HCOOH and HCHO (Figure 6d). When these liquid hydrogen carriers decompose, H_2 can be released at high yields. This process effectively breaks the C–C bonds of common biopolyols and sugars, converting them into liquid hydrogen carriers. In addition, the study demonstrated the feasibility of photocatalytic reactions directly using solar energy, enabling from the conversion of glucose into liquid hydrogen carriers. Overall, this study provides a new pathway for hydrogen production from biomass and demonstrates the potential of photocatalytic reactions in the field of sustainable energy.[70]

6. Photocatalytic H_2 Production Coupling with Alcohol Oxidation

In the photocatalytic process of overall water splitting, the O_2 evolution half–reaction is slow due to thermodynamic and kinetic limitations, which affects the overall reaction process. Adding sacrificial agents is a common strategy is to consume photogenerated holes to improve the H_2 production rate. Instead of being consumed by scavengers, photogenerated holes can be utilized to produce valuable–added products through the coupling of selective organic reactions, and realize the full utilization of electrons and holes.

6.1. Methanol Oxidation

When methanol is used as a hole sacrificial agent in H_2 production, it will be oxidized to formaldehyde, which further decomposes into CO_2 or CO. Formaldehyde is an important chemical, which is used in the processing of plastics, paints, etc. The industrial production of formaldehyde needs to catalyze methanol oxidation at high temperatures, which requires a lot of energy consumption. The co–production of formaldehyde and H_2 can be selectively achieved by photocatalysis.

Photocatalysis technology can greatly alleviate the drawbacks of the traditional methanol reforming reaction, including harsh conditions and high energy consumption.[77] However, most of the current photocatalysts have the problem of low efficiency. Karol et al. designed atomically dispersed Cu on TiO_2 composite nanoparticles with high activity and selectivity in methanol solutions. This system exhibits an apparent quantum efficiency of 10 % at 365 nm, while all the carbon is trapped in the downstream liquid mixture of formaldehyde and formic acid, making the process completely sustainable and clean.[77c] Recently, single–atom catalysis has emerged as a promising strategy to maximize the utilization of metal atoms by adjusting the atomic configuration, resulting in high efficiency and high product selectivity.[78] Tang et al. successfully loaded monatomic Cu and nanodot Pt onto the surface of TiO_2. The synergistic effect between monatom and nanodot promoted the H_2 production from methanol and water and improved the stability (Figure 7a). The results show that PtCu–TiO_2 photocatalyst exhibits excellent catalytic performance, with an H_2 yield reaching 2383.9 $\mu mol\,h^{-1}$ at 365 nm wavelength, and an AQY of 99.2 %. In addition, the PtCu–TiO_2 photocatalyst also shows high selectivity and stability, which can selectively oxidize methanol to formaldehyde, with almost no CO_2 is produced. The results also reveal the electron transport mechanism of the PtCu–TiO_2 photocatalyst, in which Cu^{2+} acts as a bridge for photoelectrons to transport to Pt, thereby driving the proton reduction reaction. In summary, this study realizes efficient, selective and stable methanol conversion through the synergistic effect of Pt nanodots and atomic Cu, providing an important idea for the design of atomic catalysts.[79]

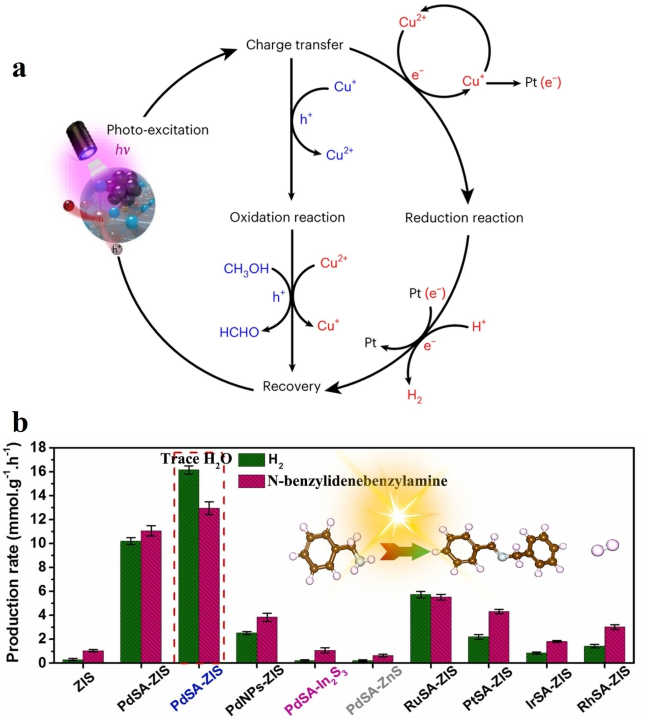

Figure 7. (a) The potential mechanism of PtCu–TiO_2 photocatalysis for the conversion of methanol and water into H_2 and valuable chemicals. Reprinted with permission.[79] Copyright 2023, Springer Nature. (b) Photocatalytic performances of N–benzylidenebenzylamine and H_2 coupling production for metal single atom–ZIS. Reprinted with permission.[82] Copyright 2022, Elsevier.

6.2. Benzyl Alcohol Oxidation

Benzaldehyde is an important industrial ingredient in the manufacture of medicine and spices, which is usually obtained by the oxidation of benzyl alcohol. However, traditional synthesis methods of benzaldehyde often require strong and harmful oxidants (e.g., $K_2Cr_2O_7$, V_2O_5 and $KMnO_4$), and high temperature and pressure conditions, which will inevitably raise production expenses and pollute the environment.[80] Therefore, the photocatalytic selective oxidation of benzyl alcohol to benzaldehyde, alongside the efficient H_2 production through water reduction, holds significant industrial potential.

The introduction of nitrogen vacancy (V_N) defects in g-C_3N_4 structure is an effective strategy to improve photocatalytic performance. V_N defects are crucial for regulating electronic structure, broadening the spectrum of light absorption, and promoting charge separation. The V_N defects can also lead to the formation of coordination–unsaturated atoms, providing active sites that can selectively adsorb and activate targeted molecules. Based on the above, Li et al. prepared a multiphase photocatalyst (Ru/g-C_3N_4-x) with metal Ru site and V_N defect double active site through a photoinduction method. In the process of photoinduced synthesis, the photogenerated electrons of g-C_3N_4 reduced Ru^{3+} to Ru nanoparticles and deposited them onto g-C_3N_4. The photogenerated holes produced free radicals that catalyzed the emergence of V_N defects on the g-C_3N_4 surface. Ru/g-C_3N_4 catalyst oxidated benzyl alcohol into benzaldehyde selectively with the rate of 5.07 $mmol\,g^{-1}\,h^{-1}$, simultaneously accompanied with H_2 production (6.42 $mmol\,g^{-1}\,h^{-1}$) The Ru/g-C_3N_4-x interface facilitates photogenerated charge separation and concurrently offers an ideal active site for both H_2 production and selective oxidation of benzyl alcohol.[81]

The single atom supported photocatalyst can also be applied to the coupling of H_2 with other organic reactions. Wang et al. designed and synthesized Pd atomically dispersed on $ZnIn_2S_4$ for simultaneous gneration of H_2 and benzylamine oxide. A single Pd atom can regulate the charge polarization of $ZnIn_2S_4$ nanocrystals, and enhance the separation and utilization efficiency of photogenerated electron–hole pairs. In addition, Pd atoms also served as active site, facilitating the oxidation of benzylamine. Under visible light, the selectivity of the oxidation product N-benzylamine reaches 100 %, with H_2 production rate of 11.1 $mmol\,g^{-1}\,h^{-1}$ (Figure 7b).[82]

7. Photocatalytic H_2 Production Coupling with Pollutants Treatment

Integrating photocatalytic H_2 production with the treatment of pollutants like plastic waste and sewage offers a sustainable solution that tackles environmental concerns and energy needs simultaneously. Photocatalytic processes can degrade plastics into less harmful substances, mitigating the pollution they cause in landfills and oceans. In wastewater treatment, these processes can oxidize and neutralize a wide range of contaminants, such as pharmaceutical residues, leading to cleaner water that can be safely returned to the environment. This dual purpose application of photocatalysis not only contributes to the circular economy by reducing waste but also aids in the transition to a more sustainable energy future by generating hydrogen, a clean and versatile fuel.

7.1. Plastics Degradation

Plastic (such as polylactic acid (PLA), polyethylene terephthalate (PET), polyurethane (PUR),) products are extensively utilized as an essential component of our everyday routines, but the majority of plastics are not biodegradable and present considerable challenges for mechanical recycling.[83] Direct landfilling results in a large number of plastic waste being discharged into the ocean, causing huge pollution to the environment.[84] Existing chemical recycling methods, including hydrolysis and pyrolysis, often require high temperatures, high pressures, and expensive catalysts, producing unnecessary greenhouse gases in the process.[85] Photocatalytic plastic reforming is an environmentally friendly and sustainable method for energy storage/conversion, which combines waste plastics with H_2 production and other organic products (such as pyruvate–based products, formate, acetate, and glycolate, etc). In this process, H_2O is reduced to H_2 by photogenerated electrons in CB, while waste plastics are oxidize into useful small molecules by holes in VB.[86] Significantly, PLA, PET, and PUR are oxygen-containing polar polymers that promote hydrolysis and subsequent photoreforming processes. In 2018, Reisner et al. proposed the technique of plastic waste photo-reforming at normal temperature as an potential method, implementing a CdS/CdO_x quantum dot catalyst that can photoreforming plastics in an alkaline solution and generate H_2.[87] Strong alkaline pretreatment is conducive to the hydrolysis of PUR and PET plastics into short chain monomers, simplifying the subsequent photoreforming reaction. The photoreforming activity of PUR reached 3.22 $mmol_{H2}\,h^{-1}\,g^{-1}$ and PET reached 12.4 $mmol_{H2}\,h^{-1}\,g^{-1}$, by simple pretreatment in NaOH aqueous solution. This is significantly higher than the previously reported Pt/TiO_2.[88] In addition, H_2 could also be produced continuously for 6 days in a real PET water bottle, with the H_2 evolution rate of 4.13 $mmol\,h^{-1}\,g^{-1}$. Although CdS/CdO_x can efficiently use visible light for photocatalytic reactions, there is still room for improvement in reaction efficiency. The shallow VB position of CdS results in a weak capacity to oxidize plastics. Deepening the VB position is a key consideration for efficient plastic degradation and H_2 evolution. The optimization of the photocatalytic process can be significantly enhanced by modulating the band structure of the $Cd_xZn_{1-x}S$ solid solution through the precise control of the Cd to Zn molar ratio. Simultaneous loading of MoS_2 cocatalyst can enhance carrier separation, provide an active site for H_2 evolution, and inhibit photocorrosion.[89] In addition, 2D/2D co–catalyst/photocatalyst with strong and large heterogeneous interfaces can substantially promote the interfacial charge transfer. When 4.3wt. % MoS_2 combined with $Cd_{0.5}Zn_{0.5}S$, the highest H_2 precipitation rate was 15.90 $mmol\,h^{-1}\,g^{-1}$, and the PET bottle was finally oxidized into small organic molecules, such as formate, methanol, lactate, and ethanol.[89]

Under alkaline conditions, polyester plastics can be depolymerized into monomers through hydrolysis to accomplish high value–added conversion, but a larger proportion of polyolefin plastic products are chemically stable dominated by C–C bonds, including polyethylene (PE), polypropylene (PP) and polystyrene (PS). Qiu et al. constructed a CdS nanorods/MoS_2 heterostructure with high spatial charge separation for photocatalytic H_2 production and multiple plastic polymers (PLA, PET and PE) conversion. In this system, photogenerated electrons tend to gather on MoS_2 for the reduction of water to evolve H_2, while photogenerated holes remain on CdS side walls for the high value–added oxidation of plastics, improving the utilization of photogenerated electrons and holes. PET and PLA were depolymerized and converted to formic acid, ethylene glycol and terephthalate. For more stable polyolefin plastics (PE), they can be converted into a series of carboxylic acid compounds after a pre–treat with nitric acid (Figure 8c). This approach holds value for the reforming of chemically stable polyolefin plastics.[8c]

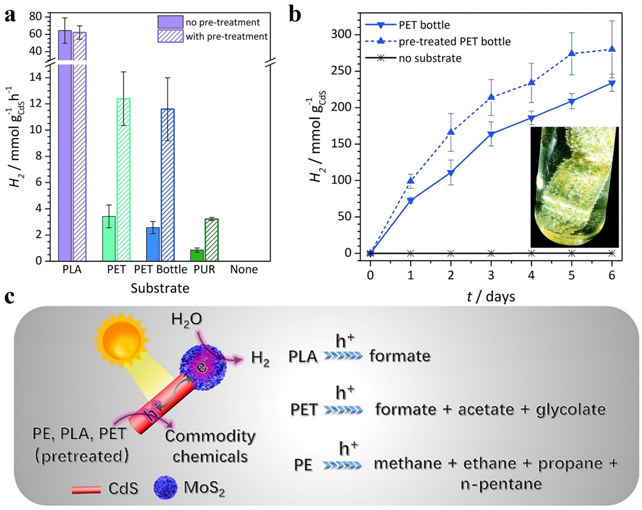

Figure 8. (a) Plastic photoreforming activity of CdS/CdO_x QDs under simulated solar light. (b) Long–term photoreforming of PET bottles to H_2 using CdS/CdO_x QDs under simulated sunlight. Reprinted with permission.[87] Copyright 2018, The Royal Society of Chemistry. (c) Schematic illustration for photoreforming of pretreated plastics over CdS nanorods with the MoS_2. Reprinted with permission.[8c] Copyright 2022, American Chemical Society.

7.2. Organic Pollutants Oxidation

Industrial wastewater often contains persistent organic pollutants that are chemically stable and resistant to biodegradation, posing serious threats to aquatic organisms and human life.[90] Using the pollutants as sacrifice agents in wastewater can achieve clean energy production and solve both energy sustainability and environmental remediation problem.[91] In the photocatalytic degradation of organic pollutants, photogenerated electrons reduce protons to produce H_2, and photogenerated holes are used to oxidize organic pollutants. The two processes of photocatalytic water splitting to produce H_2 by direct action of catalyst or through intermediate products, and photocatalytic oxidation to degrade organic pollutants are coupled together. This allows for the direct storage of the free energy generated by the degradation of organic pollutants in the form of H_2. As shown in Table 2, there have been many efforts to produce H_2 while degrading pollutants such as antibiotics and dyes in water.

To construct a photocatalytic system with high efficiency in degradating organic pollutant coupled with H_2 production, it is important to optimize the photocatalyst using different strategies. Currently reported methods include loading precious metals on the catalyst surface, doping other atoms, constructing heterojunctions, and employing heterogeneous catalysts. Xu et al. loaded Pt onto g-C_3N_4 as a catalyst to improve H_2 yield in the conversion process and reduce toxic macrolide antibiotics in the visible light system. Using the degradation process of roxithromycin as a model, HPLC-MS study confirmed that macrolide antibiotics played the role of sacrifice agents in the reaction, and realized the synergistic cooperation of degradation and coupling to produce H_2.[103] Such macrolide antibiotics exist in the form of multiple intermediates during degradation and are difficult to be completely mineralized into CO_2. A small amount of citric acid can be detected after the intermediate reaction of roxithromycin, and the pollution degree to the environment has been reduced. The design of spatial separation paths for photogenerated electrons and holes at the atomic level is an important strategy to improve the performance of single catalysts. Zhan et al. designed a Pt–doped $BaTiO_3$ with oxygen vacancy (BTPOv) monocatalyst, where the Pt–O–Ti^{3+} site serves a short charge separation site. This photocatalyst coupled moxifloxacin degradation and H_2 production, obtaining the H_2 evolution rate of 1519 $\mu mol\,g^{-1}\,h^{-1}$. Combined with experimental and DFT calculations, oxygen vacancies extracted photogenerated charges migrating from the bulk to the surface of photocatalyst. The adjacent Ti^{3+} defect allowed electrons to migrate to the Pt atom quickly via a 180° superexchange effect, with the holes confined to the Ti^{3+} defect to oxidate moxifloxstar. This work provides novel perspectives on the

Table 2: Study on the coupling reaction between photocatalytic H_2 production and degradation of organic pollutants.

Catalyst	Pollutants	H_2 Rate ($\mu mol\,h^{-1}\,g^{-1}$)	Conversion	Ref.
$Mn_{0.25}Cd_{0.75}S$/g-C_3N_4	amoxicillin	2668	98 %	[92]
ZnO/ZIS/Pt	bisphenol A	125	90.50 %	[93]
Cu atomics@UiO-66-NH_2(U_6N)/$ZnIn_2S_4$	phenol	83.4	73.10 %	[94]
Ag_3PO_4/$Cs_2AgBiBr_6$ quantum dots/graphene hydrogel	tetracycline hydrochloride	994.3	98.32 %	[95]
Pt-$BaTiO_3$	moxifloxacin	1519	98.80 %	[96]
$Sr_2MgSi_2O_7$:Eu^{2+}, Dy^{3+}/Ag_3PO_4	levofloxacin	491	81.94 %	[97]
$ZnIn_2S_4$@$CuCo_2S_4$	Ofloxacin	3200	89.40 %	[98]
	Lomefloxacin	2100	99.30 %	
	Ciprofloxacin	1900	95.70 %	
MoS_2@TiO_2	enrofloxacin	41.59	95.60 %	[99]
	Ciprofloxacin	36.82	95.30 %	
	Ofloxacin	30.26	71.10 %	
Au/TiO_2	Auramine O	10.6	44.90 %	[100]
Pt/TiO_2	Rhodamine B	33.8	79 %	
3D foaming polymeric g-C_3N_4	Tetracycline	657.9	40.30 %	[101]
TiO_2/RCN	Rhodamine B	361.8	98.60 %	[102]

synergies of multiple active sites in a single catalyst and provides a promising approach for regulating charge migration through physically–correlated effects.[96]

In addition, wang et al. constructed a $ZnIn_2S_4@CuCo_2S_4$ (ZIS@CCS) heterostructure to achieve efficient photocatalytic H_2 production from wastewater containing quinolones antibiotics. The mechanism of interfacial charge transfer was studied by system characterization and DFT calculation. When n–type ZIS and p–type CCS come into contact, the large difference in Fermi levels between them will promote carrier migration in opposite directions until the two Fermi levels reach equilibrium and the carrier migration at the interface will form an internal electric field. The p–n heterojunction system formed between ZIS and CCS promotes the separation of photogenerated carriers, creating different spaces for reduction and oxidation reactions, thus enabling both photocatalytic H_2 production and pollutant removal. In addition to the design of the catalyst, the study also suggests that the overall H_2 production rate can be increased when certain antibiotics are present in the solution. The introduction of Ofloxacin, Lomefloxacin and Ciprofloxacin into the photocatalytic system significantly increased the H_2 evolution rate. The optimal H_2 evolution rate of Ofloxacin was 0.32 $mmol\,g^{-1}\,h^{-1}$, and the degradation rate of Ofloxacin reached 89.4 % within 4 h.[98]

The discharge of dyes in wastewater is also a major pollution, compared with natural dyes, synthetic dyes are widely used because of their low production cost and flexible structure and properties. However, the discharge of dyes will pollute the water quality, hinder photosynthes and biological activities, and pose a serious threat to the water body and the entire ecosystem. Moreover, most of these dyes are chemically stable and difficult to degrade, so it is significant for the efficient treatment of organic dyes in wastewater. The most common organic dyes include methylene blue, Rhodamine B and methyl orange. For example, Yang et al. prepared a organic Z-scheme system, polydopamine/defective ultra–thin mesoporous graphite carbon nitride (PDA/DCN) for degradation of methylene blue. DFT calculations show that the defects of DCN enhance the PDA interaction, significantly polarize the internal electric field, and lead to efficient charge separation and rapid transfer. In addition, PDA enhances the photoresponse into the near-infrared range and triggers significant photothermal effects, thereby accelerating the photocatalytic reaction rate.[104] Kampouri et al. used the MOFs system for the first time to study dual photocatalysis under visible light. They systematically studied the effect of physical mixing of different transition metal–based cocatalysts with visible light active MIL-125-NH on photocatalytic water decomposition. Among them, NiO/MIL-125-NH and NisP/MIL-125-NH show a higher H_2 precipitation rate. In addition, Rhodamine B replaces the sacrificial agent and combines photocatalytic hydrogen production with RhB degradation.[105]

Although significant research has been conducted on simultaneously treating organic pollutants in wastewater and producing H_2, only a few studies have investigated the coupling of H_2 production with real or simulated wastewater treatment. More research is needed to evaluate the potential of its practical application.

8. Summary and Outlook

The coupling of photocatalytic hydrogen production with value-added reactions marks significant advances towards achieving sustainable energy and environmental amelioration by using solar energy. This review has systematically discussed the critical role of coupled photocatalytic hydrogen production, and the potential for overall water splitting, high-value chemical syntheses and pollutant degradation. This strategy provides broad application prospects in the fields of energy conversion, environmental management, and organic synthesis to achieve the win-win goals. Despite of the notable advancements, there remain several challenges limiting the development and industrialization of coupled photocatalytic H_2 production systems. The challenges and chances of future research mainly lie in the following aspects:

(1) Value

The core objective of coupled photocatalytic hydrogen production is to enhance efficiency and the comprehensive value of the reactions. Therefore, when designing the coupling reactions, it is essential to elevate the value of the oxidation half-reaction. Here, the meaning of value includes the price of the products, the energy saving for the reactions, less formation of harmful by-products in the conversion process, and the decreased burden on environment and ecology. In the future, the design of coupled photocatalytic hydrogen production reactions should not only target high-value chemicals, but also prioritize addressing challenges in various environmental contaminants and traditional industrial processes, such as those involving high temperatures and pressures, complex product separation steps, the presence of toxic by-products or intermediates. By coupling these reactions with photocatalytic hydrogen production, the costs of these processes can be reduced, and the utilization efficiency and overall value of solar energy can be improved.

(2) Photocatalyst

The photocatalyst plays the most crucial role in coupling of photocatalytic hydrogen production, primarily focusing on of light absorption, reaction efficiency, stability, and selectivity. The design of photocatalysts mainly concentrates on the band structure, charge transport channels, and surface reaction active sites for matched reactions. Some strategies have been applied to improve the performances of photocatalysts, including element doping, heterojunction construction, dye sensitization, surface modification, co-catalysts. Theoretic calculations have played an important role in the exquisite design of photocatalysts, which will continue to provide a broad range of ideas for the specific design of photocatalysts for coupling reactions. Looking ahead, the fusion of artificial intelligence and machine learning in the sphere of catalyst design and discovery is a vibrant new horizon. These advanced technologies have the capacity to expedite the development process by anticipating material behaviors and directing experimental initiatives. This could lead to a notable reduction in both the timeline and financial investment required for catalyst innovation. Future studies might consider exploring the potential of integrating these tools into photocatalyst design, with an eye towards enhancing efficiency and innovation.

(3) System

The overall design of the coupling reaction system is also a necessary condition for the successful implementation of coupled hydrogen production reactions and their transition to industrial-scale manufacturing. The construction of reaction system includes the design of the coupling reactor, the separation and collection of products, and the scaling up of the reaction process, where it is vital to consider the efficiency of the coupling reactions and ensure the safety of hydrogen gas collection. The reactor design must provide ample light exposure and maintain excellent sealing to enhance solar energy conversion efficiency and boost actual hydrogen output. Moreover, for various coupled reactions, it is crucial to refine the reaction system regarding the feedstock introduction, the separation of products from reactants, and the collection of products, to guarantee the practical application of the coupled system. Scaling up the coupled reaction system is crucial for industrialization, which may involve expanding the laboratory-scale reaction system and linking multiple smaller reaction systems to achieve large-scale production. However, in the design of the hydrogen production system, it is imperative to strictly ensure the sealing integrity of hydrogen transport pipelines and storage areas to prevent leaks that could potentially cause explosions.

In summary, although there has been considerable advancement in photocatalytic hydrogen production as a green energy technology, several challenges still need to be addressed. There is optimism that these obstacles can be surmounted with ongoing innovative research and cross-disciplinary collaboration, which would advance photocatalytic hydrogen production technology to a more sustainable and practical phase, offering a viable clean energy solution for the future.

Acknowledgements

The authors gratefully acknowledge funding support from the National Natural Science Foundation of China (22406009, U23 A20120), Natural Science Foundation of Hebei Province (B2021208033), and R&D Program of Beijing Municipal Education Commission (KZ202210005011). Derek Hao acknowledges the generous support of RMIT alumni and philanthropic contributions to the RMIT Sustainable Development Research Grants. T.M. acknowledged the Australian Research Council (ARC) through Future Fellowship (FT210100298), Discovery Project (DP220100603), Linkage Project (LP210200504, LP220100088, LP230200897) and Industrial Transformation Research Hub (IH240100009) schemes, the Australian Government through the Cooperative Research Centres Projects (CRCPXIII000077), the Australian Renewable Energy Agency (ARENA) as part of ARENA's Transformative Research Accelerating Commercialisation Program (TM021), and European Commission's Australia-Spain Network for Innovation and Research Excellence (AuSpire). Open Access publishing facilitated by RMIT University, as part of the Wiley - RMIT University agreement via the Council of Australian University Librarians.

Conflict of Interest

The authors declare no conflict of interest.

Data Availability Statement

The data that support the findings of this study are available from the corresponding author upon reasonable request.

Keywords: Photocatalysis · Hydrogen Production · Water Splitting · Coupling Reactions

---

[1] A. Kumar, P. Daw, D. Milstein, *Chem. Rev.* **2022**, *122*, 385441.

[2] a) I. Dincer, M. I. Aydin, *Energy Convers. Manage.* **2023**, *283*, 116950; b) M. Hasankhani, J. van Engelen, S. Celik, J. C. Diehl, *J. Cleaner Prod.* **2024**, *434*, 139927.

[3] a) Z. Shi, X. Zhang, X. Lin, G. Liu, C. Ling, S. Xi, B. Chen, Y. Ge, C. Tan, Z. Lai, Z. Huang, X. Ruan, L. Zhai, L. Li, Z. Li, X. Wang, G.-H. Nam, J. Liu, Q. He, Z. Guan, J. Wang, C.-S. Lee, A. R. J. Kucernak, H. Zhang, *Nature* **2023**, *621*, 300–305; b) J. Huang, B. Hu, J. Meng, T. Meng, W. Liu, Y. Guan, L. Jin, X. Zhang, *Energy Environ. Sci.* **2024**, *17*, 1007–1045.

[4] C. Wu, K. Lv, X. Li, Q. Li, *Chin. J. Catal.* **2023**, *54*, 137–160.

[5] a) P. Mazierski, A. Malankowska, M. Kobylański, M. Diak, M. Kozak, M. J. Winiarski, T. Klimczuk, W. Lisowski, G. Nowaczyk, A. Zaleska-Medynska, *ACS Catal.* **2017**, *7*, 2753–2764; b) Q. Wang, M. Nakabayashi, T. Hisatomi, S. Sun, S. Akiyama, Z. Wang, Z. Pan, X. Xiao, T. Watanabe, T. Yamada, N. Shibata, T. Takata, K. Domen, *Nat. Mater.* **2019**, *18*, 827–832.

[6] a) K. Wu, K. Li, S. Chen, Y.-J. Hou, Y.-L. Lu, J.-S. Wang, M.-J. Wei, M. Pan, C.-Y. Su, *Angew. Chem. Int. Ed.* **2020**, *59*, 2915–2915; b) X. Ma, Y. Gao, B. Yang, X. Lou, J. Huang, L. Ma, D. Jing, *Mater. Today Nano* **2023**, *21*, 100289.

[7] K. Zhang, J. Liu, L. Wang, B. Jin, X. Yang, S. Zhang, J. H. Park, *J. Am. Chem. Soc.* **2020**, *142*, 8641–8648.

[8] a) K. A. Davis, S. Yoo, E. W. Shuler, B. D. Sherman, S. Lee, G. Leem, *Nano Convergence* **2021**, *8*, 6; b) M.-Y. Qi, M. Conte, M. Anpo, Z.-R. Tang, Y.-J. Xu, *Chem. Rev.* **2021**, *121*, 13051–13085; c) M. Du, Y. Zhang, S. Kang, X. Guo, Y. Ma, M. Xing, Y. Zhu, Y. Chai, B. Qiu, *ACS Catal.* **2022**, *12*, 12823–12832.

[9] S. Lin, H. Huang, T. Ma, Y. Zhang, *Adv. Sci.* **2021**, *8*, 2002458.

[10] Q. Wang, K. Domen, *Chem. Rev.* **2019**, 120.

[11] L. Lin, T. Hisatomi, S. Chen, T. Takata, K. Domen, *Trends Chem.* **2020**, *2*, 813–824.

[12] a) S. Nishioka, F. E. Osterloh, X. Wang, T. E. Mallouk, K. Maeda, *Nat. Rev. Method. Prime.* **2023**, *3*, 42; b) S. Chen, C. Li, K. Domen, F. Zhang, *Joule* **2023**, *7*, 2445–2467.

[13] S. K. Lakhera, A. Rajan, R. T. P, N. Bernaurdshaw, *Renew. Sust. Energy Rev.* **2021**, *152*, 111694.

[14] S. Cao, T.-S. Chan, Y.-R. Lu, X. Shi, B. Fu, Z. Wu, H. Li, K. Liu, S. Alzuabi, P. Cheng, M. Liu, T. Li, X. Chen, L. Piao, *Nano Energy* **2020**, *67*, 104287.

[15] I. Monte-Pérez, S. Kundu, A. Chandra, K. E. Craigo, P. Chernev, U. Kuhlmann, H. Dau, P. Hildebrandt, C. Greco, C. Van Stappen, N. Lehnert, K. Ray, *J. Am. Chem. Soc.* **2017**, *139*, 15033–15042.

[16] A. Solé-Daura, Y. Benseghir, M.-H. Ha-Thi, M. Fontecave, P. Mialane, A. Dolbecq, C. Mellot-Draznieks, *ACS Catal.* **2022**, *12*, 9244–9255.

[17] a) J. Liu, X. Zheng, L. Pan, X. Fu, S. Zhang, S. Meng, S. Chen, *Appl. Catal. B* **2021**, *298*, 120619; b) Q. Wang, K. Domen, *Chem. Rev.* **2020**, *120*, 919–985.

[18] R. Shen, C. Qin, L. Hao, X. Li, P. Zhang, X. Li, *Adv. Mater.* **2023**, *35*, 2305397.

[19] Y. Shao, X. Hao, S. Lu, Z. Jin, *Chem. Eng. J.* **2023**, *454*, 140123.

[20] X. Chen, J. Wang, Y. Chai, Z. Zhang, Y. Zhu, *Adv. Mater.* **2021**, *33*, 2007479.

[21] X. Yan, M. Xia, H. Liu, B. Zhang, C. Chang, L. Wang, G. Yang, *Nat. Commun.* **2023**, *14*, 1741.

[22] D. Zhao, Y. Wang, C.-L. Dong, Y.-C. Huang, J. Chen, F. Xue, S. Shen, L. Guo, *Nat. Energy* **2021**, *6*, 388–397.

[23] J. Liu, Y. Liu, N. Liu, Y. Han, X. Zhang, H. Huang, Y. Lifshitz, S.-T. Lee, J. Zhong, Z. Kang, *Science* **2015**, *347*, 970–974.

[24] X. Chen, R. Shi, Q. Chen, Z. Zhang, W. Jiang, Y. Zhu, T. Zhang, *Nano Energy* **2019**, *59*, 644–650.

[25] Y. Wang, W. Huang, S. Guo, X. Xin, Y. Zhang, P. Guo, S. Tang, X. Li, *Adv. Energy Mater.* **2021**, *11*, 2102452.

[26] T. Takata, J. Jiang, Y. Sakata, M. Nakabayashi, N. Shibata, V. Nandal, K. Seki, T. Hisatomi, K. Domen, *Nature* **2020**, *581*, 411–414.

[27] Q. Wang, T. Hisatomi, Q. Jia, H. Tokudome, M. Zhong, C. Wang, Z. Pan, T. Takata, M. Nakabayashi, N. Shibata, Y. Li, I. D. Sharp, A. Kudo, T. Yamada, K. Domen, *Nat. Mater.* **2016**, *15*, 611–615.

[28] U. Kerketta, H. Kim, N. Denisov, P. Schmuki, *Adv. Energy Mater.* **2024**, *14*, 2302998.

[29] Y. Akinaga, T. Kawawaki, H. Kameko, Y. Yamazaki, K. Yamazaki, Y. Nakayasu, K. Kato, Y. Tanaka, A. T. Hanindriyo, M. Takagi, T. Shimazaki, M. Tachikawa, A. Yamakata, Y. Negishi, *Adv. Funct. Mater.* **2023**, *33*, 2303321.

[30] W. A. Qureshi, X. Hong, X. He, Q. Liu, D. Xu, C. Maouche, Z. Sun, J. Yang, *Chemosphere* **2022**, *291*, 132987.

[31] J. H. Shah, B. Huang, A. M. Idris, Y. Liu, A. S. Malik, W. Hu, Z. Zhang, H. Han, C. Li, *Small* **2020**, *16*, 2003361.

[32] W. Chen, B. Yang, Q. Yu, L. Mao, Z. Fan, Q. Wang, W. Shangguan, *Appl. Surf. Sci.* **2015**, *355*, 1069–1074.

[33] a) A. J. Bard, *J. Photochem.* **1979**, *10*, 59–75; b) B.-J. Ng, L. K. Putri, X. Y. Kong, Y. W. Teh, P. Pasbakhsh, S.-P. Chai, *Adv. Sci.* **2020**, *7*, 1903171.

[34] Y. Qi, J. Zhang, Y. Kong, Y. Zhao, S. Chen, D. Li, W. Liu, Y. Chen, T. Xie, J. Cui, C. Li, K. Domen, F. Zhang, *Nat. Commun.* **2022**, *13*, 484.

[35] Y. Sasaki, H. Nemoto, K. Saito, A. Kudo, *J. Phys. Chem. C* **2009**, *113*, 17536–17542.

[36] X. Wang, K. Maeda, A. Thomas, K. Takanabe, G. Xin, J. M. Carlsson, K. Domen, M. Antonietti, *Nat. Mater.* **2009**, *8*, 76–80.

[37] a) K. Prakash, B. Mishra, D. D. Díaz, C. M. Nagaraja, P. Pachfule, *J. Mater. Chem. A* **2023**, *11*, 14489–14538; b) S. Zhang, G. Cheng, L. Guo, N. Wang, B. Tan, S. Jin, *Angew. Chem. Int. Ed.* **2020**, *59*, 6007–6014; c) Y. Xu, N. Mao, C. Zhang, X. Wang, J. Zeng, Y. Chen, F. Wang, J.-X. Jiang, *Appl. Catal. B* **2018**, *228*, 1–9; d) Y. Yang, X. Chu, H.-Y. Zhang, R. Zhang, Y.-H. Liu, F.-M. Zhang, M. Lu, Z.-D. Yang, Y.-Q. Lan, *Nat. Commun.* **2023**, *14*, 593.

[38] K. Domen, S. Naito, T. Onishi, K. Tamaru, *Chem. Phys. Lett.* **1982**, *92*, 433–434.

[39] H. Nishiyama, T. Yamada, M. Nakabayashi, Y. Maehara, M. Yamaguchi, Y. Kuromiya, Y. Nagatsuma, H. Tokudome, S. Akiyama, T. Watanabe, R. Narushima, S. Okunaka, N. Shibata, T. Takata, T. Hisatomi, K. Domen, *Nature* **2021**, *598*, 304–307.

[40] P. Zhou, I. A. Navid, Y. Ma, Y. Xiao, P. Wang, Z. Ye, B. Zhou, K. Sun, Z. Mi, *Nature* **2023**, *613*, 66–70.

[41] a) S.-T. Xiao, R. Yin, L. Wu, S.-M. Wu, G. Tian, M. Shalom, L.-Y. Wang, Y.-T. Wang, F.-F. Pu, H.-N. Barad, F. Wang, X.-Y. Yang, *Nano Lett.* **2023**, *23*, 4390–4398; b) C. Cheng, J. Zhang, R. Zeng, F. Xing, C. Huang, *Appl. Catal. B Environ.* **2022**, *310*, 121321; c) M. Gao, P. K. N. Connor, G. W. Ho, *Energy Environ. Sci.* **2016**, *9*, 3151–3160.

[42] Y. Li, H. Zhou, S. Cai, D. Prabhakaran, W. Niu, A. Large, G. Held, R. A. Taylor, X.-P. Wu, S. C. E. Tsang, *Nat. Catal.* **2024**, *7*, 77–88.

[43] L. Li, Z. Zhou, L. Li, Z. Zhuang, J. Bi, J. Chen, Y. Yu, J. Yu, *ACS Sustainable Chem. Eng.* **2019**, *7*, 18574–18581.

[44] B. Jana, Y. Reva, T. Scharl, V. Strauss, A. Cadranel, D. M. Guldi, *J. Am. Chem. Soc.* **2021**, *143*, 20122–20132.

[45] Y. Zhong, W. Dong, S. Ren, L. Li, *Adv. Mater.* **2024**, *36*, 2308251.

[46] A. Sinhamahapatra, H.-Y. Lee, S. Shen, S. S. Mao, J.-S. Yu, *Appl. Catal. B* **2018**, *237*, 613–621.

[47] H. Li, B. Zhu, J. Sun, H. Gong, J. Yu, L. Zhang, *J. Colloid Interface Sci.* **2024**, *654*, 1010–1019.

[48] M. Gu, D.-Y. Lee, J. Mun, D. Kim, H.-i. Cho, B. Kim, W. Kim, G. Lee, B.-S. Kim, H.-i. Kim, *Appl. Catal. B* **2022**, *312*, 121379.

[49] H. Luo, Q. Guo, P. Á. Szilágyi, A. B. Jorge, M.-M. Titirici, *Trends Chem.* **2020**, *2*, 623–637.

[50] J. Lu, Y. Shi, Z. Chen, X. Sun, H. Yuan, F. Guo, W. Shi, *Chem. Eng. J.* **2023**, *453*, 139834.

[51] W. H. Lee, C. W. Lee, G. D. Cha, B.-H. Lee, J. H. Jeong, H. Park, J. Heo, M. S. Bootharaju, S.-H. Sunwoo, J. H. Kim, K. H. Ahn, D.-H. Kim, T. Hyeon, *Nat. Nanotechnol.* **2023**, *18*, 754–762.

[52] Y. Goto, T. Hisatomi, Q. Wang, T. Higashi, K. Ishikiriyama, T. Maeda, Y. Sakata, S. Okunaka, H. Tokudome, M. Katayama, S. Akiyama, H. Nishiyama, Y. Inoue, T. Takewaki, T. Setoyama, T. Minegishi, T. Takata, T. Yamada, K. Domen, *Joule* **2018**, *2*, 509–520.

[53] Y. Zhao, C. Ding, J. Zhu, W. Qin, X. Tao, F. Fan, R. Li, C. Li, *Angew. Chem. Int. Ed.* **2020**, *59*, 9653–9658.

[54] R. Ciriminna, L. Albanese, F. Meneguzzo, M. Pagliaro, *ChemSusChem* **2016**, *9*, 3374–3381.

[55] a) L. Wang, S. Cao, K. Guo, Z. Wu, Z. Ma, L. Piao, *Chin. J. Catal.* **2019**, *40*, 470–475; b) V. M. Daskalaki, P. Panagiotopoulou, D. I. Kondarides, *Chem. Eng. J.* **2011**, *170*, 433–439; c) J. Liu, Y. Zhang, L. Lu, G. Wu, W. Chen, *Chem. Commun.* **2012**, *48*, 8826–8828.

[56] J. A. Seabold, K.-S. Choi, *Chem. Mater.* **2011**, *23*, 1105–1112.

[57] D. Liu, J. Shen, Y. Xie, C. Qiu, Z. Zhang, J. Long, H. Lin, X. Wang, *ACS Sustainable Chem. Eng.* **2021**, *9*, 6380–6389.

[58] L. Zhang, W. Dong, Y. Zhang, X. Song, H. Jiang, *Chem. Eng. J.* **2023**, *472*, 144898.

[59] D. Wei, Y. Tan, Y. Wang, T. Kong, S. Shen, S. S. Mao, *Sci. Bull.* **2020**, *65*, 1389–1395.

[60] C. Hu, J. Hu, Z. Zhu, Y. Lu, S. Chu, T. Ma, Y. Zhang, H. Huang, *Angew. Chem. Int. Ed.* **2022**, *61*, e202212397.

[61] F. Chen, T. Ma, T. Zhang, Y. Zhang, H. Huang, *Adv. Mater.* **2021**, *33*, 2005256.

[62] a) J. Wang, C. Hu, Y. Zhang, H. Huang, *Chinese J. Catal.* **2022**, *43*, 1277–1285; b) C. Hu, H. Huang, F. Chen, Y. Zhang, H. Yu, T. Ma, *Adv. Funct. Mater.* **2020**, *30*, 1908168.

[63] R. M. Navarro, M. C. Sánchez-Sánchez, M. C. Alvarez-Galvan, F. d. Valle, J. L. G. Fierro, *Energy Environ. Sci.* **2009**, *2*, 35–54.

[64] a) K. Shimura, H. Yoshida, *Energy Environ. Sci.* **2011**, *4*, 2467–2481; b) Z.-X. Huang, C. Ma, F.-G. Zhang, Q. Cheng, Q.-Y. Liu, Y.-J. Yuan, X. Zhang, *J. Mater. Chem. A* **2023**, *11*, 7488–7497.

[65] S. Wang, A. Cheng, F. Liu, J. Zhang, T. Xia, X. Zeng, W. Fan, Y. Zhang, *Ind. Chem. Mater.* **2023**, *1*, 188–206.

[66] Z. Sun, G. Bottari, A. Afanasenko, M. C. A. Stuart, P. J. Deuss, B. Fridrich, K. Barta, *Nat. Catal.* **2018**, *1*, 82–92.

[67] X. Wu, S. Xie, C. Liu, C. Zhou, J. Lin, J. Kang, Q. Zhang, Z. Wang, Y. Wang, *ACS Catal.* **2019**, *9*, 8443–8451.

[68] Y. Choi, S. Choi, I. Lee, T. V. T. Nguyen, S. Bae, Y. H. Kim, J. Ryu, S. Park, J. Ryu, *Adv. Mater.* **2023**, *35*, 2301576.

[69] Z. Dou, Z. Zhang, H. Zhou, M. Wang, *Angew. Chem. Int. Ed.* **2021**, *60*, 16399–16403.

[70] P. Ren, Z. Gao, T. Montini, Z. Zhao, N. Ta, Y. Huang, N. Luo, E. Fonda, P. Fornasiero, F. Wang, *Joule* **2023**, *7*, 333–349.

[71] a) J. Zakzeski, P. C. A. Bruijnincx, A. L. Jongerius, B. M. Weckhuysen, *Chem. Rev.* **2010**, *110*, 3552–3599; b) C. Li, X. Zhao, A. Wang, G. W. Huber, T. Zhang, *Chem. Rev.* **2015**, *115*, 11559–11624.

[72] X. Wu, X. Fan, S. Xie, J. Lin, J. Cheng, Q. Zhang, L. Chen, Y. Wang, *Nat. Catal.* **2018**, *1*, 772–780.

[73] a) Z. Xu, P. Yan, H. Li, K. Liu, X. Liu, S. Jia, Z. C. Zhang, *ACS Catal.* **2016**, *6*, 3784–3788; b) K. Zhang, Z. Zhan, M. Zhu, H. Lai, X. He, W. Deng, Q. Zhang, Y. Wang, *J. Energy Chem.* **2023**, *80*, 58–67.

[74] A. A. Rosatella, S. P. Simeonov, R. F. M. Frade, C. A. M. Afonso, *Green Chem.* **2011**, *13*, 754–793.

[75] X. Bao, M. Liu, Z. Wang, D. Dai, P. Wang, H. Cheng, Y. Liu, Z. Zheng, Y. Dai, B. Huang, *ACS Catal.* **2022**, *12*, 1919–1929.

[76] S. Liu, B. Zhang, Z. Yang, Z. Xue, T. Mu, *Green Chem.* **2023**, *25*, 2620–2628.

[77] a) Z. Li, A. Ivanenko, X. Meng, Z. Zhang, *J. Hazard. Mater.* **2019**, *380*, 120822; b) M. Ran, W. Cui, K. Li, L. Chen, Y. Zhang, F. Dong, Y. Sun, *Energy Environ. Sci.* **2022**, *5*, 305–312; c) K. Ćwieka, Z. Bojarska, K. Czelej, D. Łomot, P. Dziegielewski, A. Maximenko, K. Nikiforow, L. Gradoń, M. Y. Qi, Y. J. Xu, J. C. Colmenares, *Chem. Eng. J.* **2023**, *474*, 145687.

[78] a) J. Ding, Z. Teng, X. Su, K. Kato, Y. Liu, T. Xiao, W. Liu, L. Liu, Q. Zhang, X. Ren, J. Zhang, Z. Chen, O. Teruhisa, A. Yamakata, H. Yang, Y. Huang, B. Liu, Y. Zhai, *Chem* **2023**, *9*, 1017–1035; b) H. Yin, F. Dong, D. Wang, J. Li, *ACS Catal.* **2022**, *12*, 14096–14105.

[79] H. Wang, H. Qi, X. Sun, S. Jia, X. Li, T. J. Miao, L. Xiong, S. Wang, X. Zhang, X. Liu, A. Wang, T. Zhang, W. Huang, J. Tang, *Nat. Mater.* **2023**, *22*, 619–626.

[80] W. Partenheimer, *Catal. Today* **1995**, *23*, 69–158.

[81] Q. Yang, T. Wang, Z. Zheng, B. Xing, C. Li, B. Li, *Appl. Catal. B* **2022**, *315*, 121575.

[82] P. Wang, S. Fan, X. Li, J. Wang, Z. Liu, Z. Niu, M. O. Tadé, S. Liu, *Nano Energy* **2022**, *95*, 107045.

[83] D. Pan, F. Su, C. Liu, Z. Guo, *Adv. Compos. Hybrid Mater.* **2020**, *3*, 443–461.

[84] G.-X. Wang, D. Huang, J.-H. Ji, C. Völker, F. R. Wurm, *Adv. Sci.* **2021**, *8*, 2170004.

[85] H. Dahlbo, V. Poliakova, V. Mylläri, O. Sahimaa, R. Anderson, *Waste Manage.* **2018**, *71*, 52–61.

[86] a) S. Yue, P. Wang, B. Yu, T. Zhang, Z. Zhao, Y. Li, S. Zhan, *Adv. Energy Mater.* **2023**, *13*, 2302008; b) R. Yang, G. Xu, W. Tao, Q. Wang, Y. Tang, *Green Carbon* **2024**, *2*, 1–11.

[87] T. Uekert, M. F. Kuehnel, D. W. Wakerley, E. Reisner, *Energy Environ. Sci.* **2018**, *11*, 2853–2857.

[88] T. Kawai, T. Sakata, *Chem. Lett.* **2006**, *10*, 81–84.

[89] L. Zhao, T. Dong, J. Du, H. Liu, H. Yuan, Y. Wang, J. Jia, H. Liu, W. Zhou, *Solar RRL* **2021**, *5*, 2000415.

[90] A. Kumar, A. Thakur, P. S. Panesar, *Rev. Environ. Sci. Bio.* **2019**, *18*, 153–182.

[91] L. Jiang, J. Pan, Q. Li, H. Chen, S. Zhou, Z. Yu, S. Jiang, H. Yin, J. Guan, R. A. Taylor, R. Fisher, G. Leslie, J. Scott, H. Zhao, D.-W. Wang, *EcoMat* **2022**, *4*, e12254.

[92] C. Zhang, H. Li, Y. Zhang, Y. Wang, Q. Liang, M. Zhou, S. Xu, Z. Li, *Chem. Eng. J.* **2023**, *476*, 146494.

[93] L. Yang, J. Si, L. Liang, Y. Wang, L. Zhu, Z. Zhang, *J. Colloid Interface Sci.* **2023**, *649*, 855–866.

[94] S. Liu, X. Zhou, C. Yang, C. Wei, Y. Hu, *Appl. Catal. B* **2023**, *330*, 122572.

[95] Z. Chen, X. Li, Y. Wu, A. Duan, D. Wang, Q. Yang, Y. Fan, *Sep. Purif. Technol.* **2022**, *302*, 122079.

[96] T. Zhang, Z. Zhao, D. Zhang, X. Liu, P. Wang, Y. Li, S. Zhan, *Proc. Natl. Acad. Sci. USA* **2023**, *120*, e2302873120.

[97] J. Tang, X. Liu, Y. Liu, X. Zhang, Y. Lin, L. Chen, D. Fang, J. Wang, *Chem. Eng. J.* **2022**, *435*, 134773.

[98] R. Wang, W. Yu, N. Fang, P. Wang, Y. Chu, S. Wu, J. Liang, *Appl. Catal. B* **2024**, *341*, 123284.

[99] Y. Wu, X. Chen, J. Cao, Y. Zhu, W. Yuan, Z. Hu, Z. Ao, G. W. Brudvig, F. Tian, J. C. Yu, C. Li, *Appl. Catal. B* **2022**, *303*, 120878.

[100] A. V. Puga, N. Barka, M. Imizcoz, *ChemCatChem* **2021**, *13*, 1513–1529.

[101] H. Wang, Y. Wu, M. Feng, W. Tu, T. Xiao, T. Xiong, H. Ang, X. Yuan, J. W. Chew, *Water Res.* **2018**, *144*, 215–225.

[102] H. Huang, M. He, X. Yang, Z. Tian, J. Hu, B. Wen, *Appl. Surf. Sci.* **2019**, *493*, 202–211.

[103] Z. Xu, S. Xu, N. Li, F. Wu, S. Chen, W. Lu, W. Chen, *ACS Sustainable Chem. Eng.* **2017**, *5*, 9667–9672.

[104] F. Yang, S. Wang, Z. Li, Y. Xu, W. Yang, C. Yv, D. Yang, Y. Xie, W. Zhou, *J. Colloid Interface Sci.* **2022**, *613*, 775–785.

[105] S. Kampouri, T. N. Nguyen, M. Spodaryk, R. G. Palgrave, A. Züttel, B. Smit, K. C. Stylianou, *Adv. Funct. Mater.* **2018**, *28*, 1806368.

[106] a) J. Du, B. Zhang, J. Li, B. Lai, *Chin. Chem. Lett.* **2020**, *31*, 2575–2582; b) P. Punia, M. K. Bharti, R. Dhar, P. Thakur, A. Thakur, *ChemBioEng Rev.* **2022**, *9*, 351–369.

[107] N. A. A. Qasem, R. H. Mohammed, D. U. Lawal, *NPJ Clean Water* **2021**, *4*, 36.

[108] Y. Xu, C. Zhang, P. Lu, X. Zhang, L. Zhang, J. Shi, *Nano Energy* **2017**, *38*, 494–503.

[109] Y. Liu, C. Chen, Y. He, Z. Zhang, M. Li, C. Li, X.-B. Chen, Y. Han, Z. Shi, *Small* **2022**, *18*, 2201556.

Manuscript received: August 21, 2024
Accepted manuscript online: September 20, 2024
Version of record online: October 31, 2024